Embryoid bodies facilitate comparative analysis of gene expression in humans and chimpanzees across dozens of cell types

Authors: Kenneth A Barr[1]†, Katherine L Rhodes[1]†, Yoav Gilad[1,2]*

Affiliations:

[1]Department of Medicine, University of Chicago; Chicago, IL 60637, USA.

[2]Department of Human Genetics, University of Chicago; Chicago, IL 60637, USA.

*Corresponding author. Email: gilad@uchicago.edu

†These authors contributed equally to this work

Abstract: Comparative gene expression studies in apes are fundamentally limited by the challenges associated with sampling across different tissues. Here, we used single-cell RNA-sequencing of embryoid bodies (**EBs**) to collect transcriptomic data from over 70 cell types in three humans and three chimpanzees. We found hundreds of genes whose regulation is conserved across cell types, as well as genes whose regulation likely evolves under directional selection in one or a handful of cell types. Using EBs from a human-chimpanzee fused cell line, we also inferred the proportion of inter-species regulatory differences due to changes in *cis* and *trans* elements between the species. Thus, we present the most comprehensive dataset of comparative gene expression from humans and chimpanzees to date, including a catalog of regulatory mechanisms associated with inter-species differences.

Introduction

Comparative functional genomic studies in primates reveal insight into the evolution of gene regulation and help us identify genes and pathways that are associated with species-specific traits (Anderson et al., 2020; Berthelot et al., 2018; Blake et al., 2020; Eres et al., 2019; Fair et al., 2020; Housman & Gilad, 2020; Klein et al., 2018; Mittleman et al., 2021). In particular, studies of gene expression in humans and other apes allow us to identify regulatory changes that may be associated with human-specific adaptations (Danko et al., 2018; Housman & Gilad, 2020; O'Bleness et al., 2012; Pizzollo et al., 2018). Comparative inter-species studies also allow us to identify patterns of regulatory variation that are consistent with the action of natural selection. Such patterns suggest functional importance and point to regulatory phenotypes that may affect fitness. The inference of fitness-related molecular function is profoundly important, not only to studies that attempt to understand the mechanisms of evolutionary change, but also to studies of the genetic and gene regulatory basis for complex traits and diseases in humans (Benito-Kwiecinski et al., 2021; Fair et al., 2020; Gokhman et al., 2021; Housman et al., 2022; Mittleman et al., 2021; Pizzollo et al., 2018; Pollen et al., 2019; Shibata et al., 2012; Ward & Gilad, 2019).

One goal of comparative genomic studies in primates has been to characterize gene regulatory variation across a wide range of tissue types. Comparative genomic studies are not typically hypothesis-driven; rather, they aim to build comprehensive comparative catalogs that can be used to infer function, explore the evolution of different regulatory mechanisms, and establish hypotheses based on causal inference between genotypes and phenotypes (Berthelot et al., 2018; Blake et al., 2020; Danko et al., 2018; Eres et al., 2019; Fair et al., 2020; Klein et al., 2018; Mittleman et al., 2021; Pizzollo et al., 2018). Yet, more than two decades after the first genome-scale comparison of gene expression in humans and chimpanzees (Enard et al., 2002), comparative genomic data from apes remains limited to just a handful of tissue types (Housman & Gilad, 2020).

For obvious ethical and practical reasons, only a small number of tissue types can be accessed from live humans, and direct experimentation *in vivo* is impossible. While *in vivo* studies are permitted in some primates, ethical considerations forcefully apply to studies of apes, particularly to studies involving chimpanzees – our closest extant evolutionary relatives. Comparative studies in apes must therefore rely on opportunistic collection of post-mortem tissues. Efforts to collect a broad array of post-mortem tissues from humans have been quite successful (GTEx Consortium, 2020), but comparative genomic studies in humans and chimpanzees have only examined about a dozen different tissues. Moreover, the sample size in nearly all comparative studies in apes is quite modest: most studies include just 4-6 donors from each non-human species (Barreiro et al., 2010; Blake et al., 2018, 2020; Blekhman et al., 2008, 2010; Cáceres et al., 2003; Cain et al., 2011; De la Cruz et al., 2009; Eres et al., 2019; Gilad et al., 2006; Hernando-Herraez et al., 2013; Housman et al., 2022; Iskow et al., 2012; Khan et al., 2013; Lemos et al., 2005; Mittleman et al., 2021; Pai et al., 2011; Perry et al., 2012), and in some cases, only a single sample from the non-human species was available (Brawand et al., 2011; Enard et al., 2002; Gilad et al., 2005; Hernando-Herraez et al., 2015). In the handful of comparative studies that examine more than one tissue in apes, multiple tissues are rarely sampled from the same individuals (Barbosa-Morais et al., 2012; Blekhman et al., 2008; Brawand et al., 2011; Cáceres et al., 2003; De la Cruz et al., 2009; Enard et al., 2002; Pai et al., 2011; Perry et al., 2012), resulting in a severe confounding of tissue and

individual effects on the observed variation in gene regulation (a confounding effect that is particularly severe due to the small sample size available from each tissue (Blake et al., 2020)).

Even if we had unlimited access to post-mortem frozen tissues from apes, we would still be unable to study dynamic gene regulation, let alone study how different tissues and cell types respond to environmental exposures. Induced pluripotent stem cells (**iPSCs**) from apes provide a way to study gene regulatory dynamics during differentiation or in response to external perturbations (Gallego Romero et al., 2015), but the inefficiency of differentiation protocols limits the number of individuals, cell types, and contexts that can be queried in a single experiment. Thus, the scope of comparative studies in apes has remained narrow: we are unable to study gene regulation in more than a few tissues from apes; we are generally unable to collect samples from enough individuals to map and study regulatory quantitative trait loci (**QTLs**) in non-human apes; we are unable to study the dynamics of gene regulation during development; and we are unable to study regulatory responses to evolutionarily and clinically relevant exposures.

If we are ever to unleash the power of the comparative paradigm in apes, we require an *in vitro* system that allows us to dynamically study gene regulation in dozens of different cell types and individuals, and in hundreds of different contexts. Here, we show that embryoid bodies (**EBs**) can potentially fulfill these requirements. EBs are dynamic, iPSC-derived organoids that contain spontaneously and asynchronously differentiating cells from all three germ layers (Brickman & Serup, 2017).

We recently used single-cell RNA-sequencing (**scRNA-seq**) to characterize cellular and gene expression heterogeneity in a panel of human EBs, which revealed the presence of dozens of differentiating and terminal cell types from multiple different tissues (Rhodes et al., 2022). In the present study, we applied scRNA-seq to EBs from three humans and three chimpanzees. Despite the small size of our sample, we were able to assemble a comparative catalog of gene expression data from more than 70 different cell types per species, including differentiating cell types that have never been accessible from frozen tissues. This catalog contains nearly an order of magnitude more cell types than have been examined before, and three times more comparative data from humans and chimpanzees than all previous studies combined.

Using gene expression data from EBs, we identify hundreds of genes that are differentially expressed across dozens of cell types, as well as genes that are broadly conserved. We analyze tissue-restricted patterns of differential expression between the species, implicating a handful of candidate genes that may underlie functional differences between humans and chimpanzees. In addition, we quantify the contribution of *cis* and *trans* changes to inter-species differences in gene expression using EBs derived from a fused human-chimpanzee iPSC line.

Results

Generation of human and chimpanzee embryoid bodies

We generated EBs from three human YRI (Yoruba in Ibadan, Nigeria) and three western chimpanzee iPSC lines that were previously validated (Banovich et al., 2018; Gallego Romero et al., 2015). From each line, we established EBs in three independent replicates (**Figure 1A and Figure S1**; see Materials and methods). We also included a single replicate of EBs from three additional human lines of European ancestry to confirm that inter-species differences are not population-specific.

We formed EBs in micropatterned plates and cultured them for two days before transferring them to suspension culture. On day 21, we dissociated EBs into single-cell suspensions and collected single-cell transcriptomes using 10x Genomics scRNA-seq. To prevent systematic biases in transcriptomes due to differences in genome annotation, we aligned reads to a curated set of orthologous exons in the human and chimpanzee genomes. After filtering (see Materials and methods), we retained data from 115,269 cells (a median of 5,385 cells from each replicate) in which we detected the expression of a median of 3,149 genes (**Table S1**).

We first verified the presence of cells from the three germ layers in all samples by considering the expression of *SOX17, HAND1*, and *PAX6* as markers for endoderm, mesoderm, and ectoderm, respectively (**Figure S2**). In all samples, we also identified cells expressing *POU5F1* (Oct4), indicating the presence of undifferentiated cells (iPSCs). At low resolution, we identified 11 clusters of cells using Louvain clustering in Seurat (**Figure S2A**). In all clusters, we found cells from both species, with most clusters showing a nearly even proportion of human and chimpanzee cells (**Figure S2B and Table S2**).

To identify cell types within EBs, we considered human and chimpanzee gene expression data together with previously generated reference data containing cells from EBs, human embryonic stem cells (**hESCs**), and primary fetal tissues (Cao et al., 2020; Han et al., 2020; Rhodes et al., 2022). We labeled each of our cells based on its relative position within this reference (**Figure 1B**), which allowed us to partition cells into meaningful groups for subsequent analyses. In total, we identified 86 cell types present in both human and chimpanzee EBs (77 labels transferred from the reference and nine cell types identified *de novo*; see **Table S3**). These represent undifferentiated cells, cells from each of the three germ layers, and cells that closely resemble extra-embryonic cell types (**Figure 1C**). Cells from both species are well-distributed across all cell types (**Figure 1D-E**).

Differential expression between humans and chimpanzees in 72 cell types

Next, we characterized differential expression (**DE**) between humans and chimpanzees in individual cell types. We excluded cell types that did not contain at least 5 cells in at least two replicates. We generated pseudobulk expression data for each of the remaining 72 cell types and performed DE analysis using a linear mixed model implemented in DREAM (Hoffman & Roussos, 2021). In addition to modeling the effect of species, we included random effects for replicate and individual. At a 5% false discovery rate (**FDR**), we identified DE genes in 70 cell types. Across all cell types, we identified 59,940 instances of DE genes between humans and chimpanzees; 10,457 (72% of all tested) genes are DE between the species in at least one cell type, with a range of two (chromaffin cells) to 3,712 (early ectoderm) DE genes in individual cell types (**Table S4 and Data S1**).

We explored the extent to which genes show inter-species DE in more than one cell type. To account for incomplete power to detect DE (given that we have only three individuals per species), we used Cormotif (Wei et al., 2015) to jointly analyze data from all 72 cell types simultaneously. This allowed us to share information across cell types, improving the power and accuracy of DE analysis. We identified 13 motifs of DE across cell types. At a posterior probability of 95%, we identified between 27 and 7,095 DE genes in each cell type, with a median of 2,718. 10,783 genes (74%) were DE in at least one cell type (**Table S4**). Compared to the underpowered single-tissue analysis, the mean number of cell types in which each gene was classified as DE increased from 4.1 to 14.7.

Examining the Cormotif results (**Figure 2A**), we found that the two largest classes of genes are those that are DE between species in all cell types (motif 11) and those that are not DE in any cell type (motif 1). These patterns of DE could indicate different degrees of selective constraint. Indeed, we found that the number of cell types in which a gene is classified as DE between species is significantly associated with coding sequence similarity between humans and chimpanzees (**Figure 2B**; $p = 2.7 \times 10^{-6}$). The ratio of non-synonymous to synonymous coding mutations across mammals (dN/dS) and the loss-of-function observed/expected upper bound fraction (**LOEUF**) (Karczewski et al., 2020) are also positively associated with the number of cell types in which a gene is classified as DE (**Figure 2C-D**; dN/dS $p = 10^{-13}$; LOEUF $p < 10^{-15}$). These observations are consistent with the notion that broad gene expression differences between humans and chimpanzees are generally associated with relaxation of evolutionary constraint. For a subset of broadly DE genes, it may be the case that directional selection has favored a new regulatory pattern. In support of this, we found that genes targeted by human accelerated regions (**HARs**) are also DE in a greater number of cell types (**Figure 2E**; $p = 4.6 \times 10^{-5}$).

Genes with conserved expression levels across all cell types are of particular interest, as they may shed insight on core functions in both species. Yet, the identification of these genes is confounded by statistical power. To confidently classify these genes, we filtered non-DE genes by their absolute expression levels (**Figure 2F**). We classified hundreds of non-DE genes across all cell types, even at relatively stringent filters. For example, non-DE genes with at least 100 UMIs in at least 10 cell types in both species are enriched for core cellular processes, including protein transport and mRNA processing, splicing, and transport (**Table S5**).

Beyond genes that are DE in no cell types or all cell types, many of the remaining DE motifs have tissue-specific patterns. Inter-species DE in specific tissues could be driven by tissue-specific expression patterns, where genes may be DE everywhere they are expressed. In other cases, a gene may have acquired DE in a restricted set of cell types, despite being expressed in additional cell types. To examine these possibilities, we considered the expression levels of the genes in each motif across all cell types and compared them to patterns of DE (**Figure 2G-H and Figure S3**). We focused on motifs exhibiting tissue-specific DE while the genes are highly expressed, but are conserved in other cell types. We then identified genes with cell type-restricted acquisition of DE (see Materials and methods). We identified 3,906 genes (27%) that are broadly expressed but show cell-type-specific DE between humans and chimpanzees (**Data S2**).

Tissue-restricted DE could underlie important functional differences between humans and chimpanzees. For instance, the transcription factor TCF7L2 is a WNT modulator associated with human psychiatric and metabolic disorders (del Bosque-Plata et al., 2022, p. 7). *TCF7L2* is broadly expressed in EBs, but inter-species DE is restricted to neuronal subtypes, where it may underlie inter-species differences in neurodevelopment (**Figure 2I and Figure S4A-B**). Another example is *SCG3*, an obesity-associated gene (Tanabe et al., 2007) for which inter-species DE is restricted to a few cell types, including acinar (pancreatic) cells (**Figure 2J and Figure S4C-D**). This cell-type-specific pattern could underlie inter-species differences in digestive activity.

Generation of EBs from tetraploid human chimpanzee hybrids

Next, we sought to further characterize mechanisms of inter-species DE. To quantify the contribution of *cis* versus *trans* regulatory divergence to inter-species differences in gene

expression, we sequenced single EB cells from a human-chimpanzee fused stem cell line (Agoglia et al., 2021; Gokhman et al., 2021). We generated 65,247 fused single-cell transcriptomes from three replicates. Upon mapping these cells to the reference data, we observed cells from all 86 previously identified cell types (**Figure 3A**). We identified DE genes in each cell type using a paired Wilcoxon signed-rank test. At a 5% FDR, we observed DE in 67 cell types, with 13,842 genes classified as DE in at least one cell type (**Table S4**).

Fused tetraploid cells contain the complete genome of both the human and chimpanzee parental lines; thus, genes from both species share the same *trans* environment. We estimated the proportion of gene expression divergence due to *cis* by comparing the change in gene expression observed between human and chimpanzee alleles in the tetraploid cells, to the change in gene expression observed between the original human and chimpanzee diploid cells (**Figure 3B**). Inter-species gene expression differences that cannot be explained by *cis* are assumed to be driven by changes in *trans* (though noise and measurement error will confound the *trans* estimate).

On average, we estimated that 70% of inter-species changes in gene expression are not due to changes in *trans* elements (**Figure 3C**), though as we pointed out, measurement error is expected to contribute to this estimate. Indeed, when we restrict this analysis to the 1,000 tests with the lowest error in the estimate of effect size, the proportion of *trans* regulation is decreased, as expected, to 62% (**Figure 3C**). We found that changes in *trans* elements are associated with larger effect sizes (**Figure 3D**; $p < 10^{-15}$). We generally expect *trans* changes – particularly pleiotropic changes that affect multiple cell types – to be deleterious, and therefore, rare. However, a *trans* change that affects only one cell type is more likely to persist. Consistent with this expectation, we found that *trans* changes are depleted from genes that are broadly DE between the species – that is, the number of cell types in which a gene is classified as inter-species DE is negatively correlated with the proportion of DE that is explained by differences in *trans* (**Figure 3E-F**; $p < 10^{-15}$).

We proceeded by arbitrarily classifying DE genes as *cis* if the mean estimated *cis* proportion across DE cell types was greater than 75%, or *trans* if the estimated *cis* proportion was less than 25%. We found that *cis* genes are associated with higher coding sequence divergence (**Figure 4A**; $p = 2 \times 10^{-6}$), higher dN/dS ratios (**Figure 4B**; $p = 0.01$), and higher LOEUF (**Figure 4C**; $p = 10^{-15}$) relative to *trans* genes. *Trans* genes are significantly enriched for functions related to development and morphogenesis (**Table S6**), and for many miRNA and transcription factor binding motifs (**Table S7**), the latter of which suggests a link between changes in expression and upstream regulators. For instance, *CLDN4* has a *trans* DE proportion of 93% and is a predicted target of the transcription factor *CEBPA*. Consistently, the pattern of DE across cell types for these two genes is highly correlated (**Figure 4D-E and Figure S5**; $\rho = 0.88$, $p = 0.007$).

Discussion

We used EBs to create the most comprehensive comparative catalog of gene expression levels in humans and chimpanzees to date, including single-cell data from 86 developing and mature cell types across multiple germ layers and tissues. Importantly, the EB model system allowed us to generate each of these cell types from every human and chimpanzee individual using uniform processing, such that we did not confound cell type with individual, species, or

processing method in our analysis. Our balanced study design allowed us to explore gene regulatory divergence at an unprecedentedly high cellular and temporal resolution.

We confirmed that gene regulatory divergence is ubiquitous across cell types, even in closely related species. More than two thirds of tested genes are DE in at least one cell type, and in the majority of cell types there are hundreds to thousands of DE genes between the species. We identified thousands of genes that are DE in a subset of the cell types in which these are expressed, which suggests that there are quite a few functional changes in tissue-specific gene regulation between the two species.

We were somewhat surprised to find a large subset of genes whose expression is conserved in all of the cell types we were able to study. We did not expect such a large fraction of genes to be regulated in a similar way in humans and chimpanzees in over 70 different cell types, as this requires that the regulation of these genes is of sufficient functional importance in all of these cell types to evolve under relatively strong constraint. It is of course possible that with data from more individuals, we would find that a subset of the 'generally conserved' genes are in fact DE between the species in some of the cell types; nevertheless, this observation is intriguing and suggests that we should reconsider our assumptions regarding the degree of context-specific gene regulation.

Turning our attention to regulatory mechanisms, the use of fused cell lines allowed us to assess the relative contribution of *cis* and *trans* changes to regulatory evolution – an approach that has not been feasible in primates until recently (Agoglia et al., 2021; Gokhman et al., 2021; Starr et al., 2022). We found that *cis* changes are common and can impact any number of cell types, as expected given the potential for spatial and temporal specificity of *cis* elements. Our observation that *trans* changes are associated with inter-species DE in fewer cell types than *cis* changes may seem counterintuitive, because one expects *cis* changes to be more specific than changes in *trans*. However, *trans* changes are more likely to be associated with pleiotropic deleterious outcomes than changes in *cis*. Thus, while *trans* changes are likely more exposed to negative selection, they may persist if their impact is restricted to a small number of cell types and thus drive the observed correlation between breadth of DE and proportion of *trans*.

We also found that fused lines help to identify putative regulatory relationships between genes. By combining correlated patterns of DE across cell types with binding motif enrichment in the promoters of *trans*-regulated DE genes, we demonstrated that *CEBPA* may drive tissue-specific differential expression of *CLDN4*. In principle, this approach could be used to identify key sets of *cis*-regulated genes that drive divergence in expression between humans and chimpanzees. Future studies of human-chimpanzee hybrid EBs could also explore how *cis* and *trans* differences are distributed through gene regulatory networks.

Collectively, our work validates EBs as a powerful model system for comparative studies of gene expression in humans and chimpanzees. The EB system confers several advantages over existing models. First, the use of EBs sidesteps the many pitfalls of working with frozen tissues, which have severely limited the scope of comparative studies in primates. Frozen tissues from non-human apes must be collected opportunistically, making it difficult to sample broadly across tissues, obtain samples from more than a handful of individuals per species, and design unbiased studies that are balanced with respect to species, tissue, and individual (Blake et al., 2020). Moreover, frozen tissues cannot be used to study how gene regulation changes over time or in response to external perturbations. While iPSC-derived cell types and organoids provide a way to explore gene regulatory dynamics *in vitro* (Agoglia et al., 2021; Elorbany et

al., 2022; Pollen et al., 2019; Shibata et al., 2012; Ward & Gilad, 2019), EBs can be used to efficiently generate multiple cell types with a fraction of the effort it takes to differentiate a single iPSC line. Indeed, EBs permit the study of gene regulation across dozens of cell types, individuals, developmental time points, and environmental exposures, which will allow future studies to explore gene regulatory divergence in apes in greater detail than has been possible thus far.

In particular, gene expression response phenotypes have not been widely explored in apes, even using *in vitro* models. Understanding how human and chimpanzee cells respond to external perturbations can reveal how gene regulatory divergence affects transcriptional responses that are relevant to human-specific traits and diseases, and may reveal functionally important genes and pathways that affect fitness. In a previous study, we examined the immune response to infection in primary monocytes from humans, chimpanzees, and rhesus macaques (Barreiro et al., 2010). We observed that while the regulatory response to bacterial infection is largely conserved between species, the regulatory response to viral infection is often lineage-specific. For example, we found chimpanzee-specific immune signaling pathways to be enriched for HIV-interacting genes, which could explain why HIV-infected chimpanzees exhibit relatively strong resistance to AIDS progression (Barreiro et al., 2010).

More recently, we used iPSC-derived cardiomyocytes from humans and chimpanzees to examine inter-species differences in response to hypoxia, a symptom of myocardial ischemia (Ward & Gilad, 2019). Despite differences in myocardial ischemia risk, heart development, and other cardiovascular traits between the two species, we observed that the response of human and chimpanzee cardiomyocytes to hypoxia was largely conserved. We also found that hypoxia-induced transcription factors bind more frequently to conserved hypoxia response genes than to chimpanzee-specific hypoxia response genes, suggesting that changes to transcription factors or their binding sites might underlie inter-species differences in hypoxia (and possibly, differences in myocardial infarction risk). In each of these studies, we identified functionally important genes and mechanisms by comparing the transcriptional responses of a single cell type to a disease-relevant exposure. The EB model system makes it possible to perform similar studies in dozens of cell types at once, including transient, developmental cell types that are not accessible from adult tissues.

In summary, EBs are a powerful *in vitro* model system that can be used to address a number of outstanding questions in primate comparative genomics. Our initial exploration of human and chimpanzee EBs resulted in the first comparative database of *cis* and *trans* regulatory divergence between the species, which includes gene expression data from more than 70 human and chimpanzee cell types. Future studies will take full advantage of this model by including additional human and chimpanzee cell lines, by studying how *cis* and *trans* changes interact to drive adaptation and divergence, and by exploring divergent transcriptional responses to biomedically relevant perturbations between the two species.

Materials and methods

Samples

In this study we included six human and three chimpanzee iPSC lines. The three human lines were derived from unrelated individuals from the Yoruba population in Ibadan, Nigeria (YRI) as part of the International HapMap Collection. These lines were reprogrammed from lymphoblastoid cell lines and characterized in (Banovich et al., 2018). Two of these lines are female (18511, 18858) and one is male (19160). We included three additional fibroblast-derived human iPSC cell lines characterized in (Gallego Romero et al., 2015). Two of these lines are female (H28834, H21792) and one is male (H28126). We included three fibroblast-derived chimpanzee iPSC lines, also characterized in (Gallego Romero et al., 2015). These also included two females (C40280, C3651) and one male (C3649). We obtained the tetraploid human/chimpanzee hybrid iPSC line (HLI-25) from Dr. Hunter Fraser.

iPSC maintenance

We maintained feeder-free iPSC cultures on Matrigel Growth Factor Reduced Matrix (CB-40230, Thermo Fisher Scientific) with StemFlex Medium (A3349401, Thermo Fisher Scientific) and Penicillin/Streptomycin (30002Cl, Corning). We grew cells in an incubator at 37°C, 5% CO2, and atmospheric O2. Every 3-5 days thereafter, we passaged cells to a new dish using a dissociation reagent (0.5 mM EDTA, 300 mM NaCl in PBS) and seeded cells with ROCK inhibitor Y-27632 (ab120129, Abcam).

Embryoid body formation and maintenance

We formed EBs using the STEMCELL AggreWell™400 protocol according to the manufacturer's directions. Briefly, we generated a single-cell suspension of iPSCs by incubating them for 5 to 13 minutes with 300 mM NaCl in PBS, followed by gentle pipetting. We seeded iPSCs into an AggreWell™400 24-well plate at a density of 1,000 cells per microwell. We cultured the aggregates in AggreWell™ EB Formation Medium (05893, STEMCELL) with ROCK inhibitor Y-27632 for 24 hours. After 24 hours, we replaced 1mL of the media with fresh EB Formation Medium. After another 24 hours, we harvested the EBs and placed them on an ultra-low attachment 6-well plate (CLS3471-24EA, Sigma) in E6 media (A1516401, ThermoFisher Scientific). We replaced the media every other day for the next 19 days, for a total of 21 days of EB culture.

We formed EBs on three separate days. The first day we included all six human lines and all three chimpanzee lines. For the next two experimental replicates, we included all three chimpanzee lines, but only the three YRI human lines.

Embryoid body dissociation

On day 21 post-formation, we dissociated EBs into a single-cell suspension. We washed the cells in PBS (Corning 21-040-CV) and then incubated them in 1mL of AccuMax dissociation reagent (STEMCELL 7921) for 10 minutes at 37°C. After 10 minutes, we gently pipetted the EBs for 30 seconds using a clipped p1000 tip. We repeated this every five minutes until we achieved a single-cell suspension, up to a maximum of 35 minutes. Next, we stopped dissociation by adding 5mL of ice-cold E6 media. We then filtered cells using a 40um strainer (Fisherbrand 22-363-547). We washed the cells three times using ice-cold PBS + 0.04% BSA. Prior to running the cells on the

10X Chromium controller, we mixed the cells together, including an equal number of cells from each individual.

Library preparation and sequencing

We generated scRNA-seq libraries using the 10X Genomics 3' scRNA-seq v3.0 kit. We targeted 10,000 cells per lane of the 10X chip. In the first replicate, with nine individuals, we initially collected nine lanes (~90,000 cells). For the remaining two replicates we collected four lanes (~40,000 cells). We performed all sequencing using 100bp paired-end sequencing on a HiSeq 4000 at the University of Chicago Functional Genomics Core Facility. We initially pooled and replicated libraries 1-2 and 6-9 and sequenced on one lane, and pooled libraries 1 and 3-5 on another lane. Our preliminary analysis indicated that library 2 was poor quality and we excluded it from further analyses. Libraries 3, 4, and 5 contained fewer cells than expected, but otherwise appeared to be good quality. We re-pooled the eight remaining libraries using half the amount of libraries 3-5 to account for lower library complexity. We sequenced this pool on eight lanes of the HiSeq 4000. We also pooled and sequenced libraries from replicates 2 and 3 on one lane each of the HiSeq 4000. After preliminary analysis, we performed an additional six and four lanes of sequencing on the HiSeq400 for replicate 2 and replicate 3 libraries, respectively. For each replicate, the number of sequencing lanes was chosen such that we obtained 50% saturation as assessed by 10X cellranger software.

Orthologous exon reference generation

In order to make quantitative comparisons across species that are not biased by differences in mapping annotation quality across species, we generated a database of orthologous exons. We followed the general approach of (Blekhman et al., 2010; Pavlovic et al., 2018) but updated this database to use the most recent version of the chimpanzee genome assembly (Clint_PTRv2/panTro6). Briefly, we mapped the human genome annotation (hg38/Ensembl98) onto the chimpanzee genome using three separate BLAT steps. First, we used BLAT on every protein-coding human exon to identify the ortholog in chimpanzee. We kept exons that had at least 80% sequence identity. For exons with multiple locations at greater than 80% sequence identity, we retained the exon that shared the most neighboring exons (within 100 kb) with the original reference. We also removed exons with indels greater than 20% of the exon length. Next, we used BLAT to map these chimpanzee exons back to the human genome. We retained exons mapped back to their original location in human. Finally, we used BLAT to the map the chimpanzee exons to the chimpanzee genome. We retained exons that map back to the original location in chimpanzee. The resulting reference contains 1,077,831 orthologous exons from 19,787 genes.

Alignment, species assignment, demultiplexing, filters and normalization of human and chimpanzee libraries

We compiled three separate references using the cellranger *mkref* command from 10x Genomics: one human, one chimpanzee, and one combined human and chimpanzee reference. Each reference was generated using the appropriate species annotation from the orthologous exon database described above. We used cellranger count to map reads to each of these three references. We used the combined genome reference to assign species to each barcode. We assigned a cell barcode to a species if greater than 90% of uniquely mapping reads mapped to that species' genome.

We used demuxlet to assign each droplet to an individual (Kang et al., 2018). We used genotypes for NA19160, NA18858 and NA18511 from the 1000 genomes project (Consortium, 2012). Genotypes for human and chimpanzee individuals H21792, H28126, C3649, C3651, and C40280

were obtained from Dr. Gregory Wray. We generated genotype calls for the remaining individual, H28834, using RNA-sequencing data from (Blake et al., 2018) and the GATK best-practices pipeline for calling genotypes from sequencing data.

We filtered the data to remove droplets that had fewer than 1,000 genes detected. We also removed droplets where mitochondrial reads represented more than 20% of total reads or fewer than 0.1% of total reads. We processed the data using the SCTransform pipeline from Seurat (Hafemeister & Satija, 2019) using 5,000 variable genes and obtained Pearson residuals for all genes.

Reference integration and cell type assignment of human and chimpanzee cells

We have previously reported a joint reference containing cells from human EBs (Rhodes et al., 2021) as well as cells from a fetal cell atlas (Cao et al., 2020) and human embryonic stem cells (**hESCs**) (Han et al., 2020). We mapped the human and chimpanzee cells onto this reference. Briefly, we embedded the human and chimpanzee cells in the PCA space of the joint reference. Next, we used Harmony (Korsunsky et al., 2019) to correct the PCs of the human and chimpanzee datasets while holding the reference PCs fixed.

In order to assign cell type identities from the fetal cell reference, we first assigned cluster midpoints (by taking the mean of each harmony-corrected PC) for each cell type in the fetal cell atlas as well as hESCs. We then assigned a cell identity to each cell in the human and chimpanzee EB dataset by finding the closest reference cluster midpoint by Euclidean distance. This resulted in a substantial number of cells that were assigned to hESCs, meaning they more closely resembled undifferentiated cells than anything within the fetal reference. These cells represent both undifferentiated cells and immature or transient developing cell types not present in either reference. To assign identities to these cells, we performed unsupervised clustering using the Louvain algorithm (in Seurat, using resolution 0.1). This resulted in 9 new cell types. We then reassigned every human and chimpanzee EB cell using the fetal cell reference midpoints, as well as midpoints for each of these 9 *de novo* cell types.

Alignment, filters, normalization, and cell type assignment of hybrid libraries

We performed two separate alignments of the tetraploid human-chimpanzee hybrid cell lines using cellranger count. We aligned all of the data to the standard human reference (2020-A, obtained from 10x Genomics) as well as the combined orthologous exon reference described above. We used the human-aligned data to filter, normalize, integrate with the reference, and assign cell identities. We removed droplets that had fewer than 2,000 genes detected, as well as droplets with fewer than 0.1% or more than 20% of reads aligning to mitochondrial genes. We processed the data using SCTransform with 5,000 variable genes, returning residuals for all genes. Using the procedure described above, we then aligned our data with the joint reference, including all human and chimpanzee data generated in this study. We assigned each hybrid cell the identity of the nearest reference cell by Euclidean distance in Harmony-corrected PC space.

We used data aligned to the combined human and chimpanzee reference for all quantitative comparisons. By default, cellranger discards sequencing reads that do not uniquely map to the genome. Therefore, reads that remain after alignment represent fragments that can be uniquely assigned to the allele of one species. We retained droplets that passed filters in the human-aligned data. We also transferred relevant metadata, including cell type identities, from the human-aligned data.

***Differential expression between humans and chimpanzees with* DREAM**

In order to perform differential expression (**DE**) analysis, we generated pseudo-bulk expression by taking the sum of counts for all cells that came from the same individual, replicate, and cell type. We than removed any samples with 5 or fewer cells. For each cell type, we filtered genes using the *filterByExpr* function from the R package edgeR(Robinson et al., 2010), setting the variable *min.count* to 5. We performed DE analysis using DREAM (Hoffman & Roussos, 2021) separately in each cell type, setting species as a fixed effect and individual and replicate as random effects. We estimated size factors using trimmed mean of M-values (**TMM**) with singleton pairing and we performed cyclic loess normalization.

***Joint differential expression with* Cormotif**

The package Cormotif (Wei et al., 2015) uses *t*-statistics from LIMMA (Smyth, 2004), performed in multiple conditions, to share information and improve power of DE analysis. The software takes normalized gene expression measurements as input. This may be inappropriate for single-cell RNA-sequencing projects, where the number of cells per sample may vary by more than an order of magnitude. We modified the Cormotif package to accept UMI counts as input. To generate *t*-statistics, our modified package runs limma-voom (Law et al., 2014) in order to apply precision weights to each sample. We used the same gene filters as we used for DREAM. We also used TMM and cyclic loess normalizations. The modified Cormotif package that implements this is available on github at https://github.com/kennethabarr/CormotifCounts.

Identification of cell type restricted differential expression

To visualize the expression patterns of genes within correlation motifs, we generated a motif score for each motif in each cell. For each motif, we first took the product of the SCTtransform residuals for each gene and the probability that each gene is a member of that motif. We then summed these motif membership-weighted SCTransform residuals for all genes. We then computed z-scores of this metric to visualize distributions of motif expression.

To identify single genes with tissue-restricted patterns of DE, we first filtered for genes with greater than 95% posterior probability of DE in at least one cell type. Within this set, we identified genes that had posterior of probability of DE of less than 5% in at least one cell type. To ensure that differential power could not explain the lack of DE in the conserved cell type, we required that the conserved cell type have at least 100 total observed UMIs for that gene in both humans and chimpanzees.

Differential expression in tetraploid hybrid cells

For every gene and cell type, we performed a paired Wilcoxon signed rank test to compare the within-cell difference between counts of reads assigned to human alleles vs chimpanzee alleles. We used the row_wilcoxon_paired function from the matrixTests package to implement this (Koncevičius, 2021). We then adjusted p-values within each cell type using the Benjamini-Hochberg procedure (Benjamini & Hochberg, 1995).

Estimates of* cis *proportions

To estimate the relative contribution of allele-specific changes (*cis* changes) to human and chimpanzee gene expression divergence, we compared the effect size between humans and chimpanzees to the effect size within tetraploid hybrid cells where the *trans* environment is fixed. We used the procedure outlined in (Agoglia et al., 2021; Gokhman et al., 2021). Briefly, we compute the *cis* component as the absolute value of the log2 fold change between humans and chimpanzees measured in hybrid cells, which we denote abs(hybrid.logFC). The *trans* and non-genetic component is the absolute value log2 fold change between humans and chimpanzees

measured in human and chimpanzee cells, minus the *cis* component. For this we used the effect size estimate computed by DREAM. We denote the *trans* and non-genetic component as abs(dream.logFC – hybrid.logFC). Thus, the *cis* proportion is given by abs(hybrid.logFC) / (abs(hybrid.logFC) + abs(dream.logFC – hybrid.logFC)).

External data sources

We obtained percent coding identity between humans and chimpanzees from BioMart (Kinsella et al., 2011). Mammalian dN/dS was obtained from a study of 29 mammalian genomes (Lindblad-Toh et al., 2011). LOEUF was obtained from a study of 141,456 human genomes (Karczewski et al., 2020). Human accelerated regions and their targets were obtained from a recently compiled set of 3,171 regions (Girskis et al., 2021).

Gene ontology and gene set enrichment

We performed gene ontology analysis using the R package topGO (Alexa & Rahnenfuhrer, 2022). We used the Fisher exact test as the statistic, and set the nodeSize parameter to 10. We performed gene set enrichments using the package *fgsea* (Korotkevich et al., 2021), with the eps parameter set to 0. We obtained gene sets from the Molecular Signature Database (MSigDB v7.5.1) (Liberzon et al., 2011). For gene set enrichment of genes generally regulated in *trans*, we ranked genes based on the mean *trans* proportion across all cell types in which each gene was DE. We provided this ranking as input to *fgsea* and used the positive score type.

Statistics

For all correlations reported in the main text, we computed p-values using Spearman's rank-order correlation test, implemented in R with the function corr.test with option method='s'. For all comparisons of the difference between distributions, we computed p-values using the two-sided Mann–Whitney *U* test, computed in R with the function wilcox.test.

References

Agoglia, R. M., Sun, D., Birey, F., Yoon, S.-J., Miura, Y., Sabatini, K., Pașca, S. P., & Fraser, H. B. (2021). Primate cell fusion disentangles gene regulatory divergence in neurodevelopment. *Nature*, *592*(7854), 421–427. https://doi.org/10.1038/s41586-021-03343-3

Alexa, A., & Rahnenfuhrer, J. (2022). *topGO: Enrichment Analysis for Gene Ontology* (2.46.0) [Computer software]. Bioconductor version: Release (3.14). https://doi.org/10.18129/B9.bioc.topGO

Anderson, J. A., Vilgalys, T. P., & Tung, J. (2020). Broadening primate genomics: New insights into the ecology and evolution of primate gene regulation. *Current Opinion in Genetics & Development*, *62*, 16. https://doi.org/10.1016/j.gde.2020.05.009

Banovich, N. E., Li, Y. I., Raj, A., Ward, M. C., Greenside, P., Calderon, D., Tung, P. Y., Burnett, J. E., Myrthil, M., Thomas, S. M., Burrows, C. K., Romero, I. G., Pavlovic, B. J., Kundaje, A., Pritchard, J. K., & Gilad, Y. (2018). Impact of regulatory variation across human iPSCs and differentiated cells. *Genome Research*, *28*(1), 122–131. https://doi.org/10.1101/gr.224436.117

Barbosa-Morais, N. L., Irimia, M., Pan, Q., Xiong, H. Y., Gueroussov, S., Lee, L. J., Slobodeniuc, V., Kutter, C., Watt, S., Colak, R., Kim, T., Misquitta-Ali, C. M., Wilson, M. D., Kim, P. M., Odom, D. T., Frey, B. J., & Blencowe, B. J. (2012). The evolutionary

landscape of alternative splicing in vertebrate species. *Science (New York, N.Y.)*, *338*(6114), 1587–1593. https://doi.org/10.1126/science.1230612

Barreiro, L. B., Marioni, J. C., Blekhman, R., Stephens, M., & Gilad, Y. (2010). Functional comparison of innate immune signaling pathways in primates. *PLoS Genetics*, *6*(12), e1001249–e1001249. PubMed. https://doi.org/10.1371/journal.pgen.1001249

Benito-Kwiecinski, S., Giandomenico, S. L., Sutcliffe, M., Riis, E. S., Freire-Pritchett, P., Kelava, I., Wunderlich, S., Martin, U., Wray, G. A., McDole, K., & Lancaster, M. A. (2021). An early cell shape transition drives evolutionary expansion of the human forebrain. *Cell*, *184*(8), 2084-2102.e19. https://doi.org/10.1016/j.cell.2021.02.050

Benjamini, Y., & Hochberg, Y. (1995). Controlling the False Discovery Rate: A Practical and Powerful Approach to Multiple Testing. *Journal of the Royal Statistical Society: Series B (Methodological)*, *57*(1), 289–300. https://doi.org/10.1111/j.2517-6161.1995.tb02031.x

Berthelot, C., Villar, D., Horvath, J. E., Odom, D. T., & Flicek, P. (2018). Complexity and conservation of regulatory landscapes underlie evolutionary resilience of mammalian gene expression. *Nature Ecology & Evolution*, *2*(1), 152–163. https://doi.org/10.1038/s41559-017-0377-2

Blake, L. E., Roux, J., Hernando-Herraez, I., Banovich, N. E., Perez, R. G., Hsiao, C. J., Eres, I., Cuevas, C., Marques-Bonet, T., & Gilad, Y. (2020). A comparison of gene expression and DNA methylation patterns across tissues and species. *Genome Research*, *30*(2), 250–262. https://doi.org/10.1101/gr.254904.119

Blake, L. E., Thomas, S. M., Blischak, J. D., Hsiao, C. J., Chavarria, C., Myrthil, M., Gilad, Y., & Pavlovic, B. J. (2018). A comparative study of endoderm differentiation in humans and chimpanzees. *Genome Biology*, *19*(1), 162. https://doi.org/10.1186/s13059-018-1490-5

Blekhman, R., Marioni, J. C., Zumbo, P., Stephens, M., & Gilad, Y. (2010). Sex-specific and lineage-specific alternative splicing in primates. *Genome Research*, *20*(2), 180–189. https://doi.org/10.1101/gr.099226.109

Blekhman, R., Oshlack, A., Chabot, A. E., Smyth, G. K., & Gilad, Y. (2008). Gene regulation in primates evolves under tissue-specific selection pressures. *PLoS Genetics*, *4*(11), e1000271. https://doi.org/10.1371/journal.pgen.1000271

Brawand, D., Soumillon, M., Necsulea, A., Julien, P., Csárdi, G., Harrigan, P., Weier, M., Liechti, A., Aximu-Petri, A., Kircher, M., Albert, F. W., Zeller, U., Khaitovich, P., Grützner, F., Bergmann, S., Nielsen, R., Pääbo, S., & Kaessmann, H. (2011). The evolution of gene expression levels in mammalian organs. *Nature*, *478*(7369), 343–348. https://doi.org/10.1038/nature10532

Brickman, J. M., & Serup, P. (2017). Properties of embryoid bodies. *Wiley Interdisciplinary Reviews. Developmental Biology*, *6*(2). https://doi.org/10.1002/wdev.259

Cáceres, M., Lachuer, J., Zapala, M. A., Redmond, J. C., Kudo, L., Geschwind, D. H., Lockhart, D. J., Preuss, T. M., & Barlow, C. (2003). Elevated gene expression levels distinguish human from non-human primate brains. *Proceedings of the National Academy of Sciences of the United States of America*, *100*(22), 13030–13035. https://doi.org/10.1073/pnas.2135499100

Cain, C. E., Blekhman, R., Marioni, J. C., & Gilad, Y. (2011). Gene expression differences among primates are associated with changes in a histone epigenetic modification. *Genetics*, *187*(4), 1225–1234. https://doi.org/10.1534/genetics.110.126177

Cao, J., O'Day, D. R., Pliner, H. A., Kingsley, P. D., Deng, M., Daza, R. M., Zager, M. A., Aldinger, K. A., Blecher-Gonen, R., Zhang, F., Spielmann, M., Palis, J., Doherty, D., Steemers, F. J., Glass, I. A., Trapnell, C., & Shendure, J. (2020). A human cell atlas of

fetal gene expression. *Science*, *370*(6518), eaba7721. https://doi.org/10.1126/science.aba7721

Consortium, T. 1000 G. P. (2012). An integrated map of genetic variation from 1,092 human genomes. *Nature*, *491*(7422), 56–65. https://doi.org/10.1038/nature11632

Danko, C. G., Choate, L. A., Marks, B. A., Rice, E. J., Wang, Z., Chu, T., Martins, A. L., Dukler, N., Coonrod, S. A., Tait Wojno, E. D., Lis, J. T., Kraus, W. L., & Siepel, A. (2018). Dynamic evolution of regulatory element ensembles in primate CD4+ T cells. *Nature Ecology & Evolution*, *2*(3), 537–548. https://doi.org/10.1038/s41559-017-0447-5

De la Cruz, O., Blekhman, R., Zhang, X., Nicolae, D., Firestein, S., & Gilad, Y. (2009). A signature of evolutionary constraint on a subset of ectopically expressed olfactory receptor genes. *Molecular Biology and Evolution*, *26*(3), 491–494. https://doi.org/10.1093/molbev/msn294

del Bosque-Plata, L., Hernández-Cortés, E. P., & Gragnoli, C. (2022). The broad pathogenetic role of TCF7L2 in human diseases beyond type 2 diabetes. *Journal of Cellular Physiology*, *237*(1), 301–312. https://doi.org/10.1002/jcp.30581

Elorbany, R., Popp, J. M., Rhodes, K., Strober, B. J., Barr, K., Qi, G., Gilad, Y., & Battle, A. (2022). Single-cell sequencing reveals lineage-specific dynamic genetic regulation of gene expression during human cardiomyocyte differentiation. *PLoS Genetics*, *18*(1), e1009666. https://doi.org/10.1371/journal.pgen.1009666

Enard, W., Khaitovich, P., Klose, J., Zöllner, S., Heissig, F., Giavalisco, P., Nieselt-Struwe, K., Muchmore, E., Varki, A., Ravid, R., Doxiadis, G. M., Bontrop, R. E., & Pääbo, S. (2002). Intra- and interspecific variation in primate gene expression patterns. *Science (New York, N.Y.)*, *296*(5566), 340–343. https://doi.org/10.1126/science.1068996

Eres, I. E., Luo, K., Hsiao, C. J., Blake, L. E., & Gilad, Y. (2019). Reorganization of 3D genome structure may contribute to gene regulatory evolution in primates. *PLoS Genetics*, *15*(7), e1008278. https://doi.org/10.1371/journal.pgen.1008278

Fair, B. J., Blake, L. E., Sarkar, A., Pavlovic, B. J., Cuevas, C., & Gilad, Y. (2020). Gene expression variability in human and chimpanzee populations share common determinants. *ELife*, *9*, e59929. https://doi.org/10.7554/eLife.59929

Gallego Romero, I., Pavlovic, B. J., Hernando-Herraez, I., Zhou, X., Ward, M. C., Banovich, N. E., Kagan, C. L., Burnett, J. E., Huang, C. H., Mitrano, A., Chavarria, C. I., Friedrich Ben-Nun, I., Li, Y., Sabatini, K., Leonardo, T. R., Parast, M., Marques-Bonet, T., Laurent, L. C., Loring, J. F., & Gilad, Y. (2015). A panel of induced pluripotent stem cells from chimpanzees: A resource for comparative functional genomics. *ELife*, *4*, e07103. https://doi.org/10.7554/eLife.07103

Gilad, Y., Oshlack, A., Smyth, G. K., Speed, T. P., & White, K. P. (2006). Expression profiling in primates reveals a rapid evolution of human transcription factors. *Nature*, *440*(7081), 242–245. https://doi.org/10.1038/nature04559

Gilad, Y., Rifkin, S. A., Bertone, P., Gerstein, M., & White, K. P. (2005). Multi-species microarrays reveal the effect of sequence divergence on gene expression profiles. *Genome Research*, *15*(5), 674–680. https://doi.org/10.1101/gr.3335705

Girskis, K. M., Stergachis, A. B., DeGennaro, E. M., Doan, R. N., Qian, X., Johnson, M. B., Wang, P. P., Sejourne, G. M., Nagy, M. A., Pollina, E. A., Sousa, A. M. M., Shin, T., Kenny, C. J., Scotellaro, J. L., Debo, B. M., Gonzalez, D. M., Rento, L. M., Yeh, R. C., Song, J. H. T., … Walsh, C. A. (2021). Rewiring of human neurodevelopmental gene regulatory programs by human accelerated regions. *Neuron*, *109*(20), 3239-3251.e7. https://doi.org/10.1016/j.neuron.2021.08.005

Gokhman, D., Agoglia, R. M., Kinnebrew, M., Gordon, W., Sun, D., Bajpai, V. K., Naqvi, S., Chen, C., Chan, A., Chen, C., Petrov, D. A., Ahituv, N., Zhang, H., Mishina, Y., Wysocka, J., Rohatgi, R., & Fraser, H. B. (2021). Human-chimpanzee fused cells reveal cis-regulatory divergence underlying skeletal evolution. *Nature Genetics*, *53*(4), 467–476. https://doi.org/10.1038/s41588-021-00804-3

GTEx Consortium. (2020). The GTEx Consortium atlas of genetic regulatory effects across human tissues. *Science (New York, N.Y.)*, *369*(6509), 1318–1330. https://doi.org/10.1126/science.aaz1776

Hafemeister, C., & Satija, R. (2019). Normalization and variance stabilization of single-cell RNA-seq data using regularized negative binomial regression. *Genome Biology*, *20*(1), 296. https://doi.org/10.1186/s13059-019-1874-1

Han, X., Zhou, Z., Fei, L., Sun, H., Wang, R., Chen, Y., Chen, H., Wang, J., Tang, H., Ge, W., Zhou, Y., Ye, F., Jiang, M., Wu, J., Xiao, Y., Jia, X., Zhang, T., Ma, X., Zhang, Q., … Guo, G. (2020). Construction of a human cell landscape at single-cell level. *Nature*, *581*(7808), 303–309. https://doi.org/10.1038/s41586-020-2157-4

Hernando-Herraez, I., Heyn, H., Fernandez-Callejo, M., Vidal, E., Fernandez-Bellon, H., Prado-Martinez, J., Sharp, A. J., Esteller, M., & Marques-Bonet, T. (2015). The interplay between DNA methylation and sequence divergence in recent human evolution. *Nucleic Acids Research*, *43*(17), 8204–8214. https://doi.org/10.1093/nar/gkv693

Hernando-Herraez, I., Prado-Martinez, J., Garg, P., Fernandez-Callejo, M., Heyn, H., Hvilsom, C., Navarro, A., Esteller, M., Sharp, A. J., & Marques-Bonet, T. (2013). Dynamics of DNA methylation in recent human and great ape evolution. *PLoS Genetics*, *9*(9), e1003763. https://doi.org/10.1371/journal.pgen.1003763

Hoffman, G. E., & Roussos, P. (2021). Dream: Powerful differential expression analysis for repeated measures designs. *Bioinformatics*, *37*(2), 192–201. https://doi.org/10.1093/bioinformatics/btaa687

Housman, G., Briscoe, E., & Gilad, Y. (2022). Evolutionary insights into primate skeletal gene regulation using a comparative cell culture model. *PLoS Genetics*, *18*(3), e1010073. https://doi.org/10.1371/journal.pgen.1010073

Housman, G., & Gilad, Y. (2020). Prime time for primate functional genomics. *Current Opinion in Genetics & Development*, *62*, 1. https://doi.org/10.1016/j.gde.2020.04.007

Iskow, R. C., Gokcumen, O., Abyzov, A., Malukiewicz, J., Zhu, Q., Sukumar, A. T., Pai, A. A., Mills, R. E., Habegger, L., Cusanovich, D. A., Rubel, M. A., Perry, G. H., Gerstein, M., Stone, A. C., Gilad, Y., & Lee, C. (2012). Regulatory element copy number differences shape primate expression profiles. *Proceedings of the National Academy of Sciences of the United States of America*, *109*(31), 12656–12661. https://doi.org/10.1073/pnas.1205199109

Kang, H. M., Subramaniam, M., Targ, S., Nguyen, M., Maliskova, L., McCarthy, E., Wan, E., Wong, S., Byrnes, L., Lanata, C. M., Gate, R. E., Mostafavi, S., Marson, A., Zaitlen, N., Criswell, L. A., & Ye, C. J. (2018). Multiplexed droplet single-cell RNA-sequencing using natural genetic variation. *Nature Biotechnology*, *36*(1), 89–94. https://doi.org/10.1038/nbt.4042

Karczewski, K. J., Francioli, L. C., Tiao, G., Cummings, B. B., Alföldi, J., Wang, Q., Collins, R. L., Laricchia, K. M., Ganna, A., Birnbaum, D. P., Gauthier, L. D., Brand, H., Solomonson, M., Watts, N. A., Rhodes, D., Singer-Berk, M., England, E. M., Seaby, E. G., Kosmicki, J. A., … MacArthur, D. G. (2020). The mutational constraint spectrum quantified from variation in 141,456 humans. *Nature*, *581*(7809), 434–443. https://doi.org/10.1038/s41586-020-2308-7

Khan, Z., Ford, M. J., Cusanovich, D. A., Mitrano, A., Pritchard, J. K., & Gilad, Y. (2013). Primate transcript and protein expression levels evolve under compensatory selection pressures. *Science (New York, N.Y.)*, *342*(6162), 1100–1104. https://doi.org/10.1126/science.1242379

Kinsella, R. J., Kähäri, A., Haider, S., Zamora, J., Proctor, G., Spudich, G., Almeida-King, J., Staines, D., Derwent, P., Kerhornou, A., Kersey, P., & Flicek, P. (2011). Ensembl BioMarts: A hub for data retrieval across taxonomic space. *Database: The Journal of Biological Databases and Curation*, *2011*, bar030. https://doi.org/10.1093/database/bar030

Klein, J. C., Keith, A., Agarwal, V., Durham, T., & Shendure, J. (2018). Functional characterization of enhancer evolution in the primate lineage. *Genome Biology*, *19*(1), 99. https://doi.org/10.1186/s13059-018-1473-6

Koncevičius, K. (2021). *matrixTests: Fast Statistical Hypothesis Tests on Rows and Columns of Matrices* (0.1.9.1) [Computer software]. https://CRAN.R-project.org/package=matrixTests

Korotkevich, G., Sukhov, V., Budin, N., Shpak, B., Artyomov, M. N., & Sergushichev, A. (2021). *Fast gene set enrichment analysis* (p. 060012). bioRxiv. https://doi.org/10.1101/060012

Korsunsky, I., Millard, N., Fan, J., Slowikowski, K., Zhang, F., Wei, K., Baglaenko, Y., Brenner, M., Loh, P.-R., & Raychaudhuri, S. (2019). Fast, sensitive and accurate integration of single-cell data with Harmony. *Nature Methods*, *16*(12), 1289–1296. https://doi.org/10.1038/s41592-019-0619-0

Law, C. W., Chen, Y., Shi, W., & Smyth, G. K. (2014). voom: Precision weights unlock linear model analysis tools for RNA-seq read counts. *Genome Biology*, *15*(2), R29. https://doi.org/10.1186/gb-2014-15-2-r29

Lemos, B., Meiklejohn, C. D., Cáceres, M., & Hartl, D. L. (2005). Rates of divergence in gene expression profiles of primates, mice, and flies: Stabilizing selection and variability among functional categories. *Evolution; International Journal of Organic Evolution*, *59*(1), 126–137.

Liberzon, A., Subramanian, A., Pinchback, R., Thorvaldsdóttir, H., Tamayo, P., & Mesirov, J. P. (2011). Molecular signatures database (MSigDB) 3.0. *Bioinformatics (Oxford, England)*, *27*(12), 1739–1740. https://doi.org/10.1093/bioinformatics/btr260

Lindblad-Toh, K., Garber, M., Zuk, O., Lin, M. F., Parker, B. J., Washietl, S., Kheradpour, P., Ernst, J., Jordan, G., Mauceli, E., Ward, L. D., Lowe, C. B., Holloway, A. K., Clamp, M., Gnerre, S., Alföldi, J., Beal, K., Chang, J., Clawson, H., … Kellis, M. (2011). A high-resolution map of human evolutionary constraint using 29 mammals. *Nature*, *478*(7370), 476–482. https://doi.org/10.1038/nature10530

Mittleman, B. E., Pott, S., Warland, S., Barr, K., Cuevas, C., & Gilad, Y. (2021). Divergence in alternative polyadenylation contributes to gene regulatory differences between humans and chimpanzees. *ELife*, *10*, e62548. https://doi.org/10.7554/eLife.62548

O'Bleness, M., Searles, V., Varki, A., Gagneux, P., & Sikela, J. M. (2012). Evolution of genetic and genomic features unique to the human lineage. *Nature Reviews. Genetics*, *13*(12), 853–866. https://doi.org/10.1038/nrg3336

Pai, A. A., Bell, J. T., Marioni, J. C., Pritchard, J. K., & Gilad, Y. (2011). A genome-wide study of DNA methylation patterns and gene expression levels in multiple human and chimpanzee tissues. *PLoS Genetics*, *7*(2), e1001316. https://doi.org/10.1371/journal.pgen.1001316

Pavlovic, B. J., Blake, L. E., Roux, J., Chavarria, C., & Gilad, Y. (2018). A Comparative Assessment of Human and Chimpanzee iPSC-derived Cardiomyocytes with Primary Heart Tissues. *Scientific Reports*, *8*(1), 15312. https://doi.org/10.1038/s41598-018-33478-9

Perry, G. H., Melsted, P., Marioni, J. C., Wang, Y., Bainer, R., Pickrell, J. K., Michelini, K., Zehr, S., Yoder, A. D., Stephens, M., Pritchard, J. K., & Gilad, Y. (2012). Comparative RNA sequencing reveals substantial genetic variation in endangered primates. *Genome Research*, *22*(4), 602–610. https://doi.org/10.1101/gr.130468.111

Pizzollo, J., Nielsen, W. J., Shibata, Y., Safi, A., Crawford, G. E., Wray, G. A., & Babbitt, C. C. (2018). Comparative Serum Challenges Show Divergent Patterns of Gene Expression and Open Chromatin in Human and Chimpanzee. *Genome Biology and Evolution*, *10*(3), 826–839. https://doi.org/10.1093/gbe/evy041

Pollen, A. A., Bhaduri, A., Andrews, M. G., Nowakowski, T. J., Meyerson, O. S., Mostajo-Radji, M. A., Di Lullo, E., Alvarado, B., Bedolli, M., Dougherty, M. L., Fiddes, I. T., Kronenberg, Z. N., Shuga, J., Leyrat, A. A., West, J. A., Bershteyn, M., Lowe, C. B., Pavlovic, B. J., Salama, S. R., … Kriegstein, A. R. (2019). Establishing Cerebral Organoids as Models of Human-Specific Brain Evolution. *Cell*, *176*(4), 743-756.e17. https://doi.org/10.1016/j.cell.2019.01.017

Rhodes, K., Barr, K. A., Popp, J. M., Strober, B. J., Battle, A., & Gilad, Y. (2021). *Human embryoid bodies as a novel system for genomic studies of functionally diverse cell types* (p. 2021.06.16.448714). https://doi.org/10.1101/2021.06.16.448714

Rhodes, K., Barr, K. A., Popp, J. M., Strober, B. J., Battle, A., & Gilad, Y. (2022). Human embryoid bodies as a novel system for genomic studies of functionally diverse cell types. *ELife*, *11*, e71361. https://doi.org/10.7554/eLife.71361

Robinson, M. D., McCarthy, D. J., & Smyth, G. K. (2010). edgeR: A Bioconductor package for differential expression analysis of digital gene expression data. *Bioinformatics*, *26*(1), 139–140. https://doi.org/10.1093/bioinformatics/btp616

Shibata, Y., Sheffield, N. C., Fedrigo, O., Babbitt, C. C., Wortham, M., Tewari, A. K., London, D., Song, L., Lee, B.-K., Iyer, V. R., Parker, S. C. J., Margulies, E. H., Wray, G. A., Furey, T. S., & Crawford, G. E. (2012). Extensive evolutionary changes in regulatory element activity during human origins are associated with altered gene expression and positive selection. *PLoS Genetics*, *8*(6), e1002789. https://doi.org/10.1371/journal.pgen.1002789

Smyth, G. K. (2004). Linear models and empirical bayes methods for assessing differential expression in microarray experiments. *Statistical Applications in Genetics and Molecular Biology*, *3*, Article3. https://doi.org/10.2202/1544-6115.1027

Starr, A. L., Gokhman, D., & Fraser, H. B. (2022). Accounting for cis-regulatory constraint prioritizes genes likely to affect species-specific traits. *BioRxiv*, 2022.03.29.486301. https://doi.org/10.1101/2022.03.29.486301

Tanabe, A., Yanagiya, T., Iida, A., Saito, S., Sekine, A., Takahashi, A., Nakamura, T., Tsunoda, T., Kamohara, S., Nakata, Y., Kotani, K., Komatsu, R., Itoh, N., Mineo, I., Wada, J., Funahashi, T., Miyazaki, S., Tokunaga, K., Hamaguchi, K., … Hotta, K. (2007). Functional Single-Nucleotide Polymorphisms in the Secretogranin III (SCG3) Gene that Form Secretory Granules with Appetite-Related Neuropeptides Are Associated with Obesity. *The Journal of Clinical Endocrinology & Metabolism*, *92*(3), 1145–1154. https://doi.org/10.1210/jc.2006-1808

Ward, M. C., & Gilad, Y. (2019). A generally conserved response to hypoxia in iPSC-derived cardiomyocytes from humans and chimpanzees. *ELife*, *8*, e42374. https://doi.org/10.7554/eLife.42374

Wei, Y., Tenzen, T., & Ji, H. (2015). Joint analysis of differential gene expression in multiple studies using correlation motifs. *Biostatistics*, *16*(1), 31–46. https://doi.org/10.1093/biostatistics/kxu038

Acknowledgments: We thank all members of the Gilad lab for helpful discussions, the Functional Genomics Core Facility at the University of Chicago for sequencing the RNA-seq libraries, and Natalia Gonzales for editing the manuscript.

Funding: National Institutes of Health grant R01HG010772 (YG).

Author contributions:

Conceptualization: KAB, KLR, YG

Methodology: KAB, KLR

Software: KAB

Validation: KLR, KAB

Formal analysis: KAB

Investigation: KAB, KLR

Resources: YG

Data curation: KLB

Writing – original draft: KAB, YG

Writing – review & editing: KAB, YG

Visualization: KAB

Funding acquisition: YG

Project administration: YG

Supervision: YG

Competing interests: Authors declare that they have no competing interests.

Data and materials availability: All raw and processed sequencing data generated in this study have been submitted to NCBI's Gene Expression Omnibus (GSE201516). Code generated for this project is available on GitHub (https://github.com/kennethabarr/CormotifCounts and https://github.com/kennethabarr/HumanChimp).

Figures

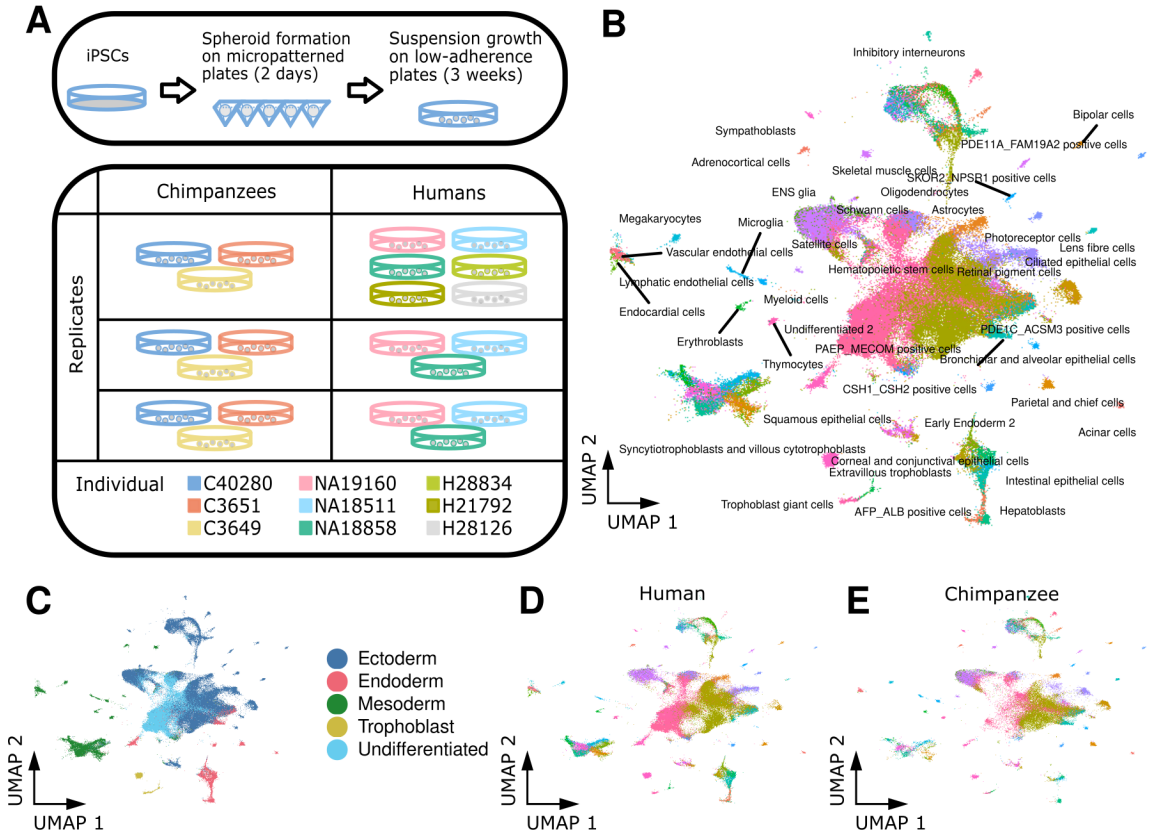

Figure 1. Human and chimpanzee embryoid bodies are composed of 86 cell types from all three germ layers. (**A**) Overview of experimental design. EBs were generated in three replicates of 6 to 9 human and chimpanzee iPSC lines. After two days in micropatterned plates, EBs were grown in low-adherence plates for 3 weeks before dissociating to single cells and sequencing with 10x scRNA-seq. (**B**) UMAP projection of all human and chimpanzee single cells after reference alignment. Cells are colored and labeled with the reference-assigned cell type. (**C**) The UMAP in (B) colored by germ layer of each cell type. The UMAP in (B) with only (**D**) human or (**E**) chimpanzee cells.

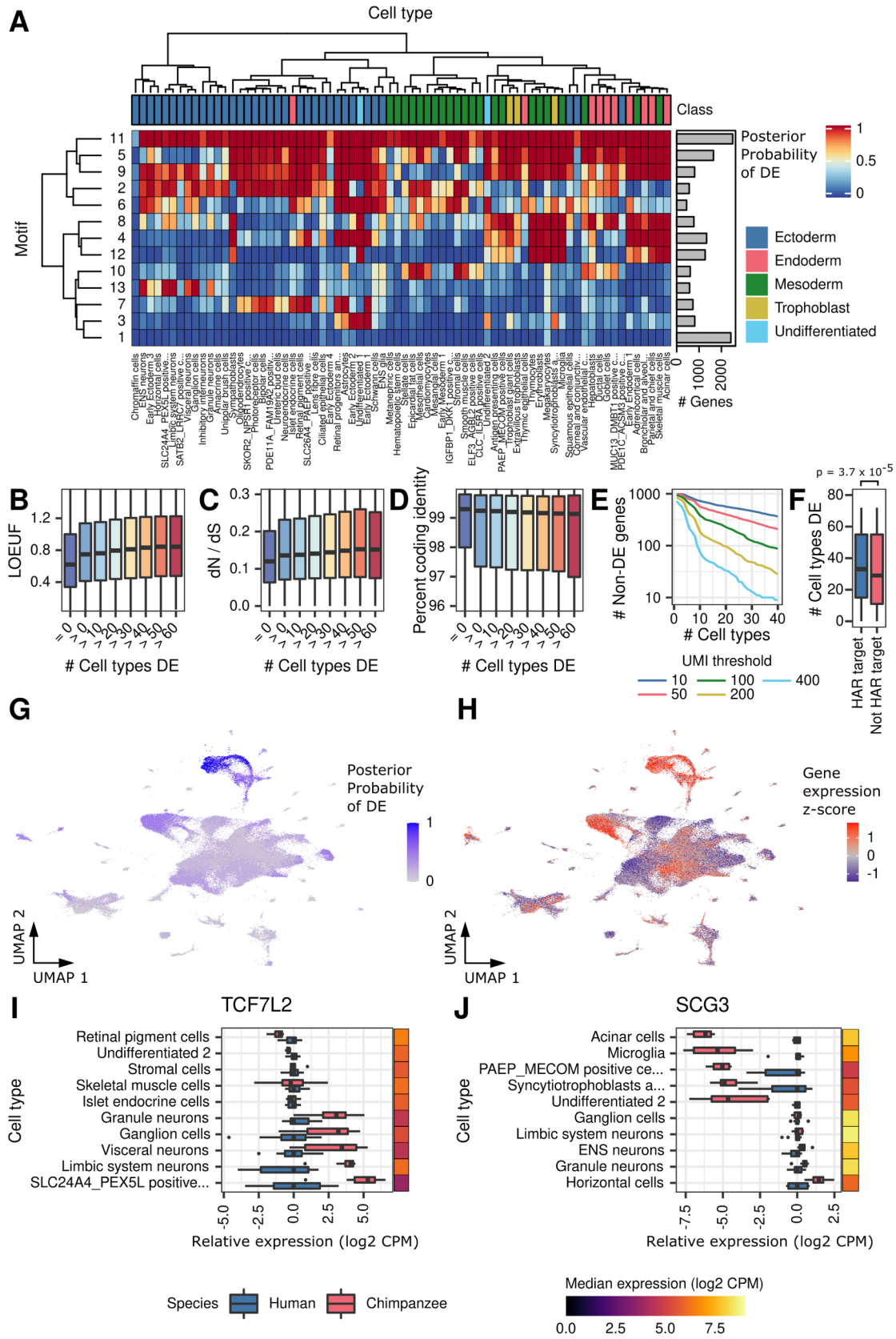
A
Cell type
Class
Motif
Posterior Probability of DE
Ectoderm
Endoderm
Mesoderm
Trophoblast
Undifferentiated
Genes
B
LOEUF
Cell types DE
C
dN / dS
Cell types DE
D
Percent coding identity
Cell types DE
E
Non-DE genes
Cell types
UMI threshold
F
Cell types DE
HAR target
Not HAR target
G
Posterior Probability of DE
UMAP 2
UMAP 1
H
Gene expression z-score
UMAP 2
UMAP 1
I
TCF7L2
Cell type
Retinal pigment cells
Undifferentiated 2
Stromal cells
Skeletal muscle cells
Islet endocrine cells
Granule neurons
Ganglion cells
Visceral neurons
Limbic system neurons
SLC24A4_PEX5L positive...
Relative expression (log2 CPM)
J
SCG3
Cell type
Acinar cells
Microglia
PAEP_MECOM positive ce...
Syncytiotrophoblasts a...
Undifferentiated 2
Ganglion cells
Limbic system neurons
ENS neurons
Granule neurons
Horizontal cells
Relative expression (log2 CPM)
Species
Human
Chimpanzee
Median expression (log2 CPM)

Figure 2. Sharing of differential expression across cell types. (**A**) Heatmap of correlation motifs across cell types. Cells are shaded according to the posterior probability of differential expression for each motif and cell type. Columns are clustered by mean gene expression. Inferred germ layers are given in **Table S3**. Boxplots of (**B**) Percent coding identity, (**C**) dN/dS, or (**D**) LOEUF in genes that are DE in zero or increasingly large numbers of cell types at posterior probability 0.5. (**E**) Boxplot showing the distribution of the number of cell types in which genes are DE for HAR targets and non-HAR target genes. (**F**) The number of non-DE genes remaining, requiring the specified absolute expression cutoffs in at least the given number of cell types. UMAP from **Figure 1B** is colored to show the (**G**) posterior probability of DE for genes in motif 13 or (**H**) the expression z-score of genes in motif 13. Boxplots show expression relative to humans in select cell types for (**I**) *TCF7L2* or (**J**) *SCG3*.

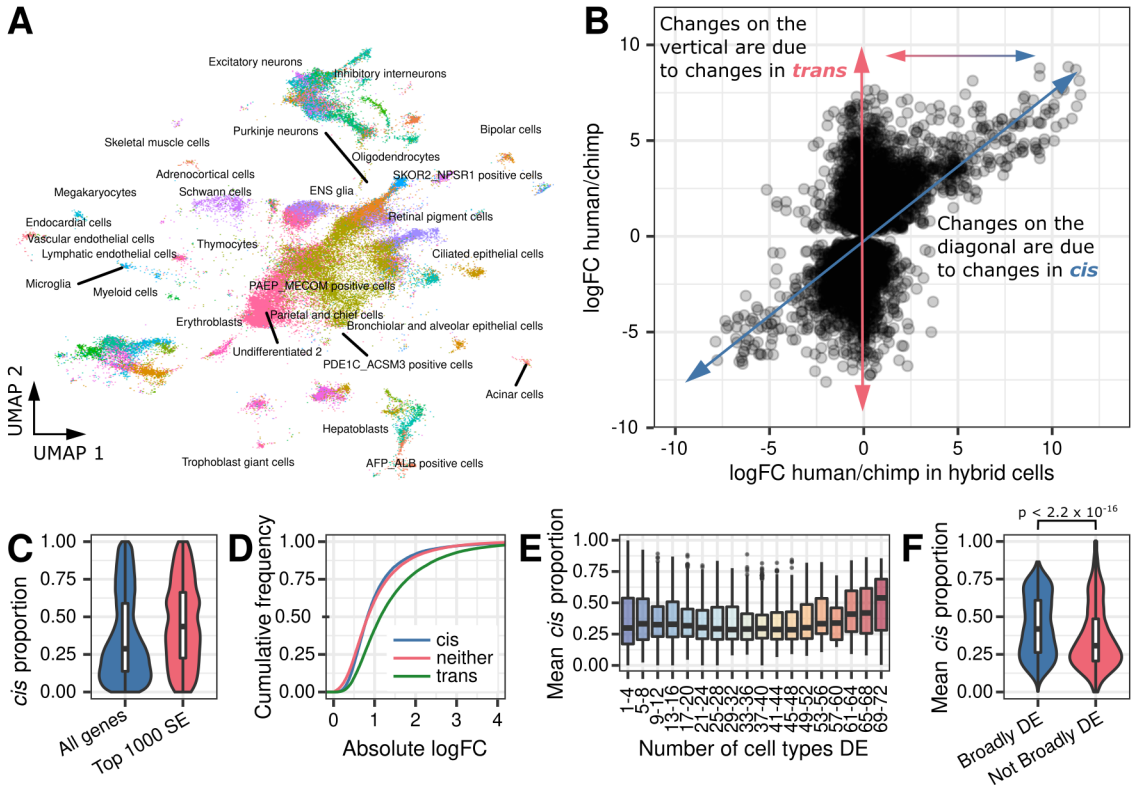

Figure 3. Allele-specific expression in tetraploid hybrid cells partitions differential expression into *cis* and *trans* components. (**A**) UMAP of hybrid cells after projection onto the space of **Figure 1B**. (**B**) The effect size in the hybrid vs. the effect size across humans and chimpanzees in DE genes ($p < 0.001$). (**C**) Boxplot of estimated *cis* proportion in the top 1,000 tests with the lowest estimate of standard error versus all other genes. (**D**) Empirical cumulative distributions of effect size (log2 fold-change from DREAM) for tests with high *cis* proportion (>0.75), low *cis* proportion (<0.25) or neither. (**E**) Boxplot of distribution of *cis* proportion for genes DE in increasingly large sets of cell types at posterior probability >95%. (**F**) Boxplot of *cis* proportion for genes DE in more than 80% of tested cell types (at posterior probability >95%) or all other genes.

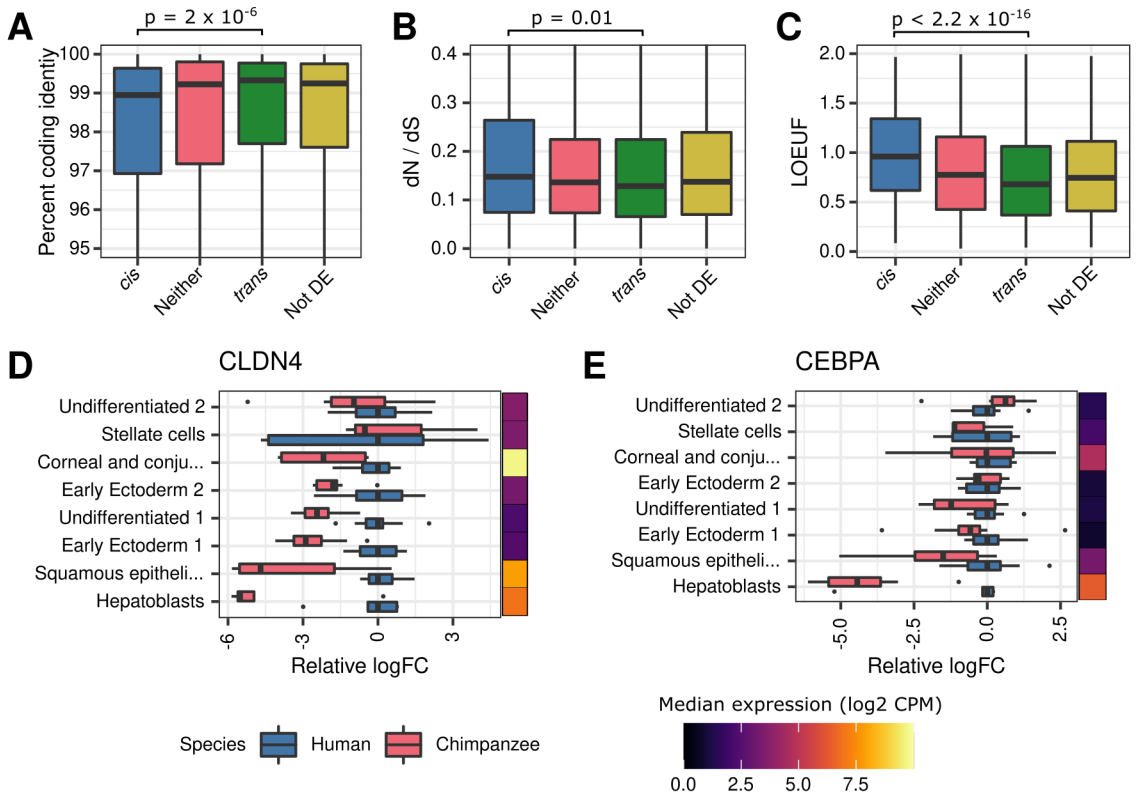

Fig 4. Genes with high *cis* proportion show evidence of relaxation of constraint. Boxplot showing the distribution of (**A**) percent coding identity (**B**) dN/dS or (**C**) LOEUF for genes with a high, moderate, or low *cis* proportion. Boxplots of showing expression relative to mean human expression in select cell types for (**D**) *CLDN4* or (**E**) *CEPBA*.

Supplementary Information and Extended Data

Figs. S1 to S5

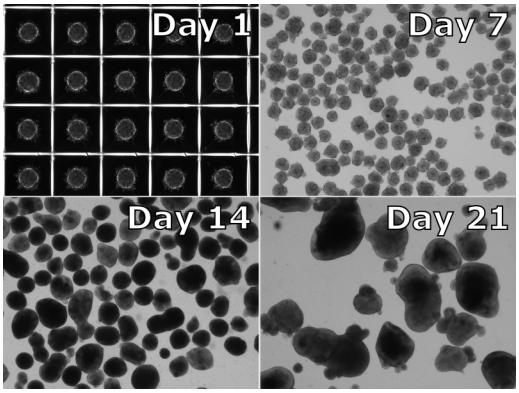

Figure S1. Representative images of embryoid bodies. Images of EBs at days 1, 7, 14, and 21 post-formation. Images are taken on an EVOS 2 FL at 4x resolution.

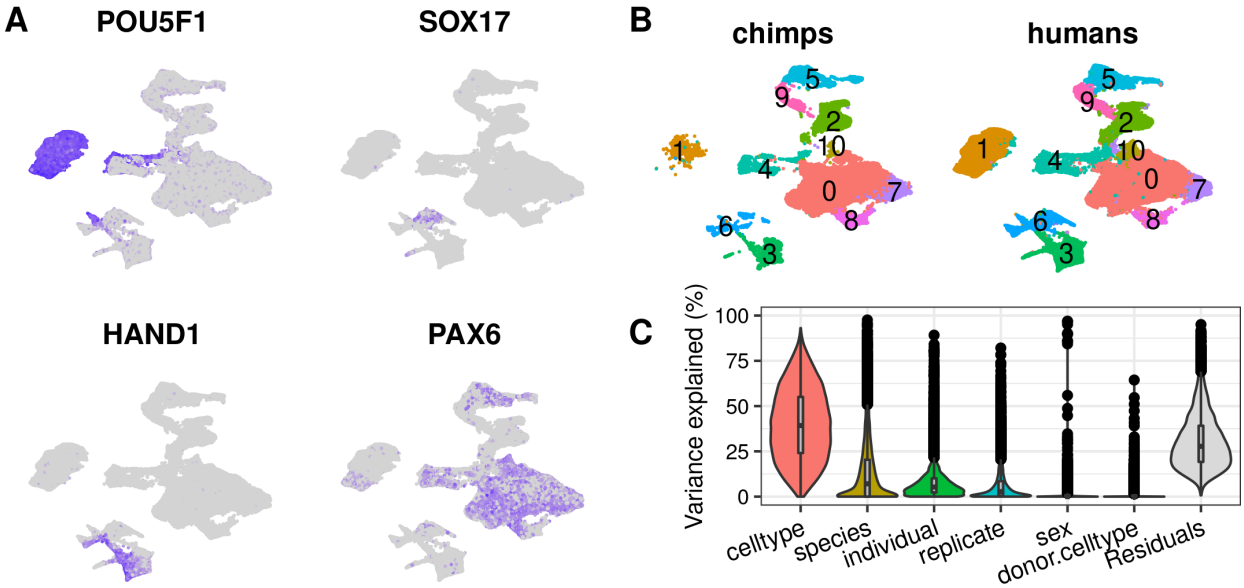

Figure S2. Cell type composition in embryoid bodies without external reference integration. (**A**) UMAP of EB cells highlighting expression of germ layer markers *POU5F1*, *SOX17*, *HAND1*, and *PAX6*. (**B**) UMAP split by species. Cells are colored by Seurat clusters at resolution 0.1. (**C**) The percent of variance explained by biological and technical factors using the VariancePartition R package.

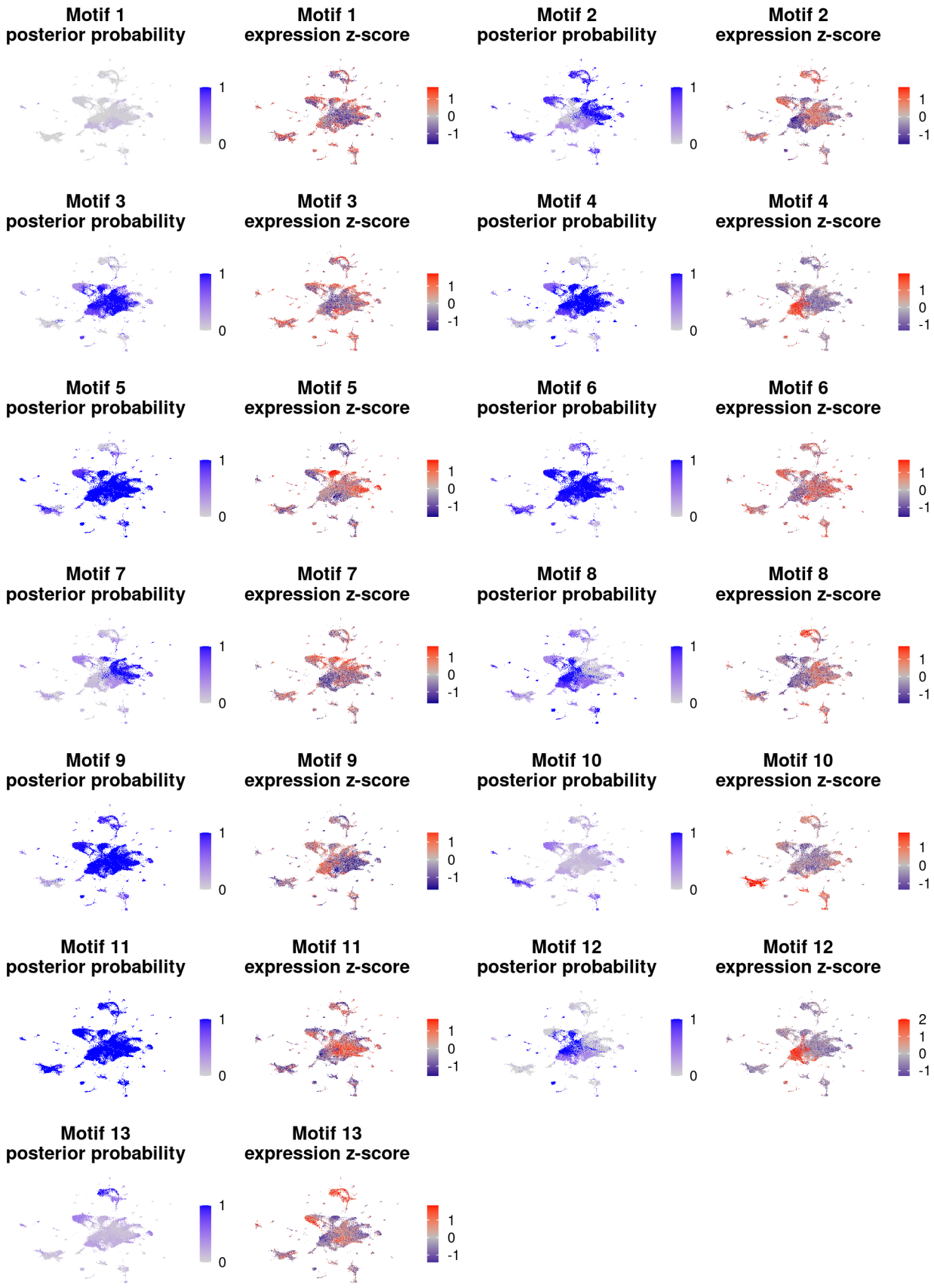
Motif 1
posterior probability
Motif 1
expression z-score
Motif 2
posterior probability
Motif 2
expression z-score
Motif 3
posterior probability
Motif 3
expression z-score
Motif 4
posterior probability
Motif 4
expression z-score
Motif 5
posterior probability
Motif 5
expression z-score
Motif 6
posterior probability
Motif 6
expression z-score
Motif 7
posterior probability
Motif 7
expression z-score
Motif 8
posterior probability
Motif 8
expression z-score
Motif 9
posterior probability
Motif 9
expression z-score
Motif 10
posterior probability
Motif 10
expression z-score
Motif 11
posterior probability
Motif 11
expression z-score
Motif 12
posterior probability
Motif 12
expression z-score
Motif 13
posterior probability
Motif 13
expression z-score

Figure S3. UMAPs of Cormotif posterior probability of differential expression and gene expression z-scores. UMAPs from **Figure 1B** with cells colored according to their posterior probability of DE or gene expression z-score (see Materials and methods).

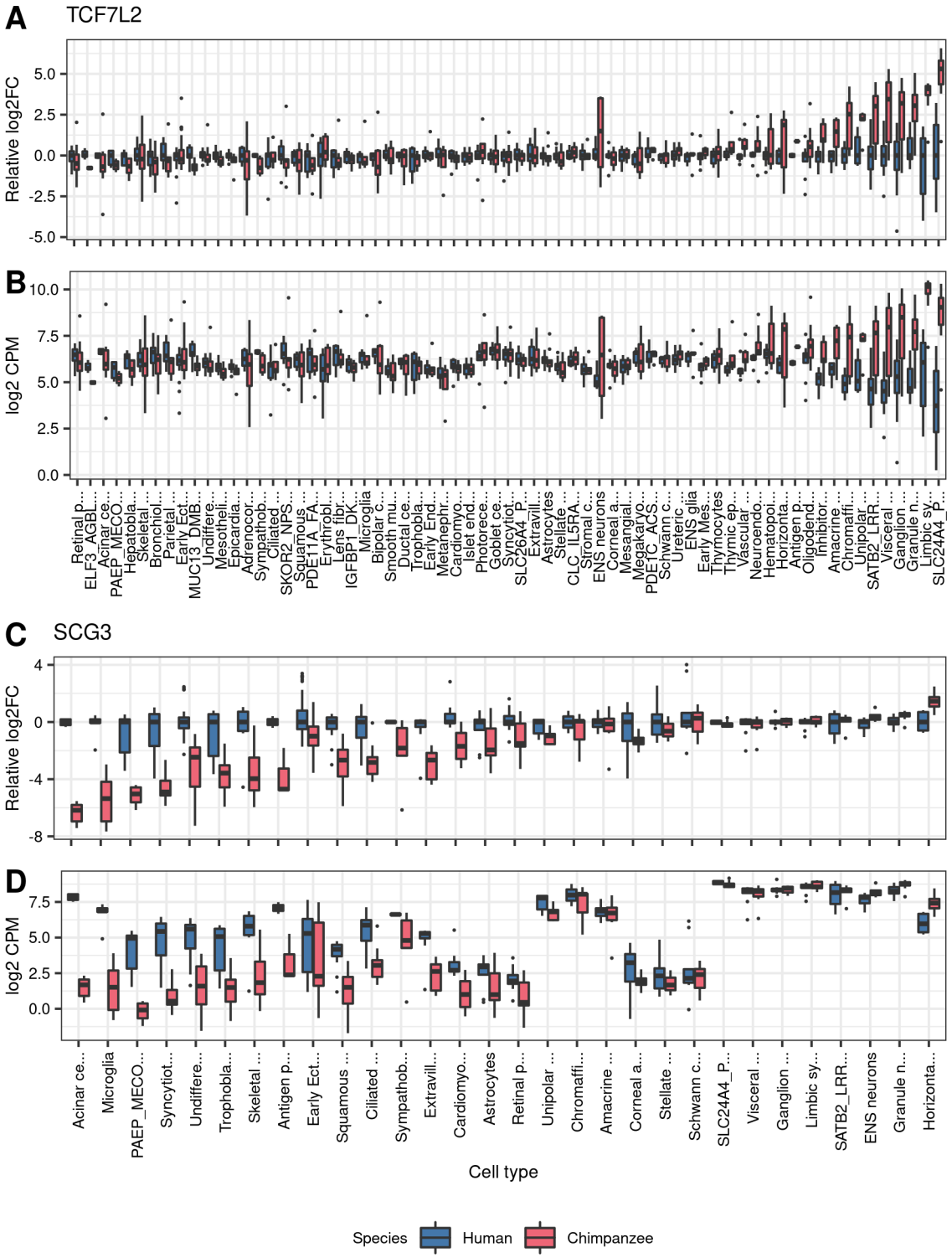

Figure S4. Boxplots of *TCF7L2* and *SCG3* expression. (**A**) Expression of *TCF7L2* in all tested cell types, relative to the mean expression in humans. (**B**) Expression of *TCF7L2* in all tested cell

types. (**C**) Expression of *SCG3* in all tested cell types, relative to the mean expression in humans. (**D**) Expression of *SCG3* in all tested cell types.

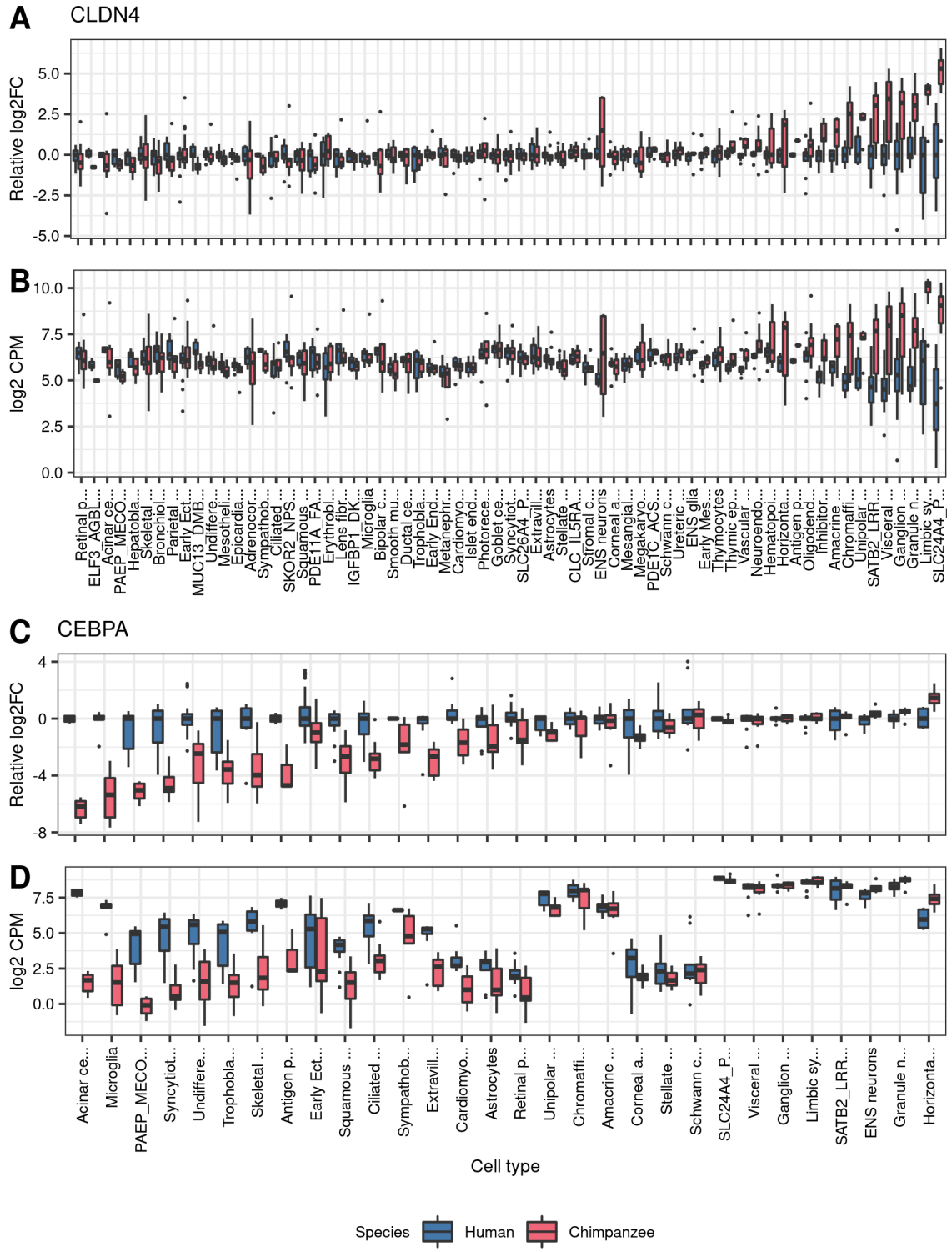

Figure S5. Boxplots of *CLDN4* and *CEBPA* expression. (**A**) Expression of *CLDN4* in all tested cell types, relative to the mean expression in humans. (**B**) Expression of *CLDN4* in all tested cell

types. (**C**) Expression of *CEBPA* in all tested cell types, relative to the mean expression in humans. (**D**) Expression of *CEBPA* in all tested cell types.

Tables S1 to S7

	Replicate1	Replicate2	Replicate3
NA19160	7921	4937	7186
NA18511	5383	5150	6068
NA18858	6805	5099	5385
H28834	5801		
H21792	5851		
H28126	5962		
C40280	3737	3569	6841
C3651	5586	4615	4652
C3649	5263	3560	5898

Table S1. Number of cells from each individual and replicate after quality control filters.

cluster	human	chimp
0	20921	24653
1	20501	398
2	4650	5931
3	7061	910
4	4106	2554
5	2119	3663
6	4702	379
7	3592	1196
8	653	2742
9	1704	1102
10	1539	193

Table S2. Number of cells from each species in each cluster without reference integration. Clusters are those defined by Seurat at resolution 0.1, and are illustrated in **Figure S2B**.

	Cell type	Germ layer	Human	Chimpanzee	Hybrid
1	Acinar cells	Endoderm	122	161	86
2	Adrenocortical cells	Mesoderm	163	145	59
3	AFP_ALB positive cells	Endoderm	465	18	384
4	Amacrine cells	Ectoderm	242	140	794
5	Antigen presenting cells	Mesoderm	57	32	19
6	Astrocytes	Ectoderm	1430	859	8000
7	Bipolar cells	Ectoderm	136	137	206
8	Bronchiolar and alveolar epithelial cells	Endoderm	187	443	168
9	Cardiomyocytes	Mesoderm	846	180	995
10	CCL19_CCL21 positive cells	Mesoderm	65	18	17
11	Chromaffin cells	Ectoderm	42	124	581
12	Ciliated epithelial cells	Ectoderm	319	723	407
13	CLC_IL5RA positive cells	Mesoderm	82	33	19
14	Corneal and conjunctival epithelial cells	Ectoderm	345	86	385
15	CSH1_CSH2 positive cells	Trophoblast	10	4	8
16	Ductal cells	Endoderm	558	129	239
17	Early Ectoderm 1	Ectoderm	14187	7751	7865
18	Early Ectoderm 2	Ectoderm	6876	6135	4491
19	Early Ectoderm 3	Ectoderm	645	469	176
20	Early Ectoderm 4	Ectoderm	99	26	132
21	Early Endoderm 1	Endoderm	537	486	1256
22	Early Endoderm 2	Endoderm	532	13	155
23	Early Mesoderm 1	Mesoderm	761	82	441
24	ELF3_AGBL2 positive cells	Mesoderm	103	40	73
25	Endocardial cells	Mesoderm	123	11	19
26	ENS glia	Ectoderm	245	611	90
27	ENS neurons	Ectoderm	649	410	229
28	Epicardial fat cells	Mesoderm	467	148	572
29	Erythroblasts	Mesoderm	143	139	52
30	Excitatory neurons	Ectoderm	18	57	530
31	Extravillous trophoblasts	Trophoblast	143	79	12
32	Ganglion cells	Ectoderm	233	365	358
33	Goblet cells	Endoderm	650	135	206
34	Granule neurons	Ectoderm	216	212	729
35	Hematopoietic stem cells	Mesoderm	166	63	132
36	Hepatoblasts	Endoderm	111	548	159
37	Horizontal cells	Ectoderm	332	143	436
38	IGFBP1_DKK1 positive cells	Mesoderm	1123	274	1237
39	Inhibitory interneurons	Ectoderm	55	108	435
40	Inhibitory neurons	Ectoderm	22	68	1190
41	Intestinal epithelial cells	Endoderm	677	15	289
42	Islet endocrine cells	Endoderm	1087	1443	403
43	Lens fibre cells	Ectoderm	73	415	89

	Celltype	Human	Chimpanzee	Hybrid
1	Acinar cells	122	161	86
2	Adrenocortical cells	163	145	59
3	AFP_ALB positive cells	465	18	384
4	Amacrine cells	242	140	794
5	Antigen presenting cells	57	32	19
6	Astrocytes	1430	859	8000
7	Bipolar cells	136	137	206
8	Bronchiolar and alveolar epithelial cells	187	443	168
9	Cardiomyocytes	846	180	995
10	CCL19_CCL21 positive cells	65	18	17
11	Chromaffin cells	42	124	581
12	Ciliated epithelial cells	319	723	407
13	CLC_IL5RA positive cells	82	33	19
14	Corneal and conjunctival epithelial cells	345	86	385
15	CSH1_CSH2 positive cells	10	4	8
16	Ductal cells	558	129	239
17	Early Ectoderm 1	14187	7751	7865
18	Early Ectoderm 2	6876	6135	4491
19	Early Ectoderm 3	645	469	176
20	Early Ectoderm 4	99	26	132
21	Early Endoderm 1	537	486	1256
22	Early Endoderm 2	532	13	155
23	Early Mesoderm 1	761	82	441
24	ELF3_AGBL2 positive cells	103	40	73
25	Endocardial cells	123	11	19
26	ENS glia	245	611	90
27	ENS neurons	649	410	229
28	Epicardial fat cells	467	148	572
29	Erythroblasts	143	139	52
30	Excitatory neurons	18	57	530
31	Extravillous trophoblasts	143	79	12
32	Ganglion cells	233	365	358
33	Goblet cells	650	135	206
34	Granule neurons	216	212	729
35	Hematopoietic stem cells	166	63	132
36	Hepatoblasts	111	548	159
37	Horizontal cells	332	143	436
38	IGFBP1_DKK1 positive cells	1123	274	1237
39	Inhibitory interneurons	55	108	435
40	Inhibitory neurons	22	68	1190
41	Intestinal epithelial cells	677	15	289
42	Islet endocrine cells	1087	1443	403
43	Lens fibre cells	73	415	89

	Cell type	Germ layer	Human	Chimpanzee	Hybrid
44	Limbic system neurons	Ectoderm	715	457	1928
45	Lymphatic endothelial cells	Mesoderm	85	5	7
46	Lymphoid cells	Mesoderm	21	7	39
47	Megakaryocytes	Mesoderm	141	430	103
48	Mesangial cells	Mesoderm	648	172	608
49	Mesothelial cells	Mesoderm	198	155	149
50	Metanephric cells	Mesoderm	532	108	216
51	Microglia	Mesoderm	278	193	140
52	MUC13_DMBT1 positive cells	Endoderm	171	170	63
53	Myeloid cells	Mesoderm	17	222	55
54	Neuroendocrine cells	Ectoderm	174	219	159
55	Oligodendrocytes	Ectoderm	187	201	1209
56	PAEP_MECOM positive cells	Mesoderm	224	95	16
57	Parietal and chief cells	Endoderm	195	196	29
58	PDE11A_FAM19A2 positive cells	Ectoderm	106	190	205
59	PDE1C_ACSM3 positive cells	Ectoderm	70	42	74
60	Photoreceptor cells	Ectoderm	179	159	91
61	Purkinje neurons	Ectoderm	3	3	62
62	Retinal pigment cells	Ectoderm	710	673	1121
63	Retinal progenitors and Muller glia	Ectoderm	2546	923	4464
64	SATB2_LRRC7 positive cells	Ectoderm	98	291	736
65	Satellite cells	Mesoderm	10	133	12
66	Schwann cells	Ectoderm	3354	3543	792
67	Skeletal muscle cells	Mesoderm	163	186	39
68	SKOR2_NPSR1 positive cells	Ectoderm	139	167	379
69	SLC24A4_PEX5L positive cells	Ectoderm	267	305	1361
70	SLC26A4_PAEP positive cells	Ectoderm	328	336	374
71	Smooth muscle cells	Mesoderm	404	157	169
72	Squamous epithelial cells	Ectoderm	523	349	1517
73	STC2_TLX1 positive cells	Mesoderm	6	1	6
74	Stellate cells	Mesoderm	531	44	397
75	Stromal cells	Mesoderm	631	293	494
76	Sympathoblasts	Ectoderm	52	118	19
77	Syncytiotrophoblasts and villous cytotrophoblasts	Trophoblast	1255	328	358
78	Thymic epithelial cells	Endoderm	559	143	413
79	Thymocytes	Mesoderm	309	200	189
80	Trophoblast giant cells	Trophoblast	228	128	116
81	Undifferentiated 1	Undifferentiated	13224	6442	4321
82	Undifferentiated 2	Undifferentiated	6048	996	7166
83	Unipolar brush cells	Ectoderm	121	153	112
84	Ureteric bud cells	Ectoderm	120	284	296
85	Vascular endothelial cells	Mesoderm	352	379	132
86	Visceral neurons	Ectoderm	284	647	1115

	Celltype	Human	Chimpanzee	Hybrid
44	Limbic system neurons	715	457	1928
45	Lymphatic endothelial cells	85	5	7
46	Lymphoid cells	21	7	39
47	Megakaryocytes	141	430	103
48	Mesangial cells	648	172	608
49	Mesothelial cells	198	155	149
50	Metanephric cells	532	108	216
51	Microglia	278	193	140
52	MUC13_DMBT1 positive cells	171	170	63
53	Myeloid cells	17	222	55
54	Neuroendocrine cells	174	219	159
55	Oligodendrocytes	187	201	1209
56	PAEP_MECOM positive cells	224	95	16
57	Parietal and chief cells	195	196	29
58	PDE11A_FAM19A2 positive cells	106	190	205
59	PDE1C_ACSM3 positive cells	70	42	74
60	Photoreceptor cells	179	159	91
61	Purkinje neurons	3	3	62
62	Retinal pigment cells	710	673	1121
63	Retinal progenitors and Muller glia	2546	923	4464
64	SATB2_LRRC7 positive cells	98	291	736
65	Satellite cells	10	133	12
66	Schwann cells	3354	3543	792
67	Skeletal muscle cells	163	186	39
68	SKOR2_NPSR1 positive cells	139	167	379
69	SLC24A4_PEX5L positive cells	267	305	1361
70	SLC26A4_PAEP positive cells	328	336	374
71	Smooth muscle cells	404	157	169
72	Squamous epithelial cells	523	349	1517
73	STC2_TLX1 positive cells	6	1	6
74	Stellate cells	531	44	397
75	Stromal cells	631	293	494
76	Sympathoblasts	52	118	19
77	Syncytiotrophoblasts and villous cytotrophoblasts	1255	328	358
78	Thymic epithelial cells	559	143	413
79	Thymocytes	309	200	189
80	Trophoblast giant cells	228	128	116
81	Undifferentiated 1	13224	6442	4321
82	Undifferentiated 2	6048	996	7166
83	Unipolar brush cells	121	153	112
84	Ureteric bud cells	120	284	296
85	Vascular endothelial cells	352	379	132
86	Visceral neurons	284	647	1115

Table S3. Number of cells from each species assigned to each reference cell type. Cell types are defined by the reference integration procedure described in Materials and methods.

	Cell Type	DREAM	CorMotif	Hybrid
1	Early Ectoderm 2	2034	6193	2034
2	Hepatoblasts	1200	3911	1200
3	Cardiomyocytes	563	2062	563
4	Syncytiotrophoblasts and villous cytotrophoblasts	3019	6359	3019
5	Schwann cells	1449	3821	1449
6	Undifferentiated 1	1682	7095	1682
7	Ciliated epithelial cells	794	3224	794
8	IGFBP1_DKK1 positive cells	278	1526	278
9	Undifferentiated 2	2073	5320	2073
10	Bipolar cells	511	2768	511
11	Metanephric cells	105	801	105
12	Trophoblast giant cells	788	4134	788
13	SLC24A4_PEX5L positive cells	350	1566	350
14	Early Ectoderm 1	3712	6709	3712
15	Squamous epithelial cells	476	3088	476
16	Retinal progenitors and Muller glia	3135	5794	3135
17	Thymocytes	1282	5115	1282
18	Astrocytes	3681	6640	3681
19	Adrenocortical cells	346	4188	346
20	Stromal cells	799	3424	799
21	Parietal and chief cells	540	4398	540
22	SKOR2_NPSR1 positive cells	463	2896	463
23	Goblet cells	1532	3139	1532
24	Mesangial cells	114	1188	114
25	Epicardial fat cells	515	2232	515
26	PDE11A_FAM19A2 positive cells	525	2536	525
27	ENS neurons	614	2280	614
28	Smooth muscle cells	367	2484	367
29	Early Ectoderm 3	492	2470	492
30	Vascular endothelial cells	993	3410	993
31	Limbic system neurons	753	2050	753
32	Early Endoderm 1	433	4791	433
33	ENS glia	516	2251	516
34	Oligodendrocytes	493	2866	493
35	Hematopoietic stem cells	105	911	105
36	Ureteric bud cells	488	2667	488
37	Visceral neurons	160	1726	160
38	PAEP_MECOM positive cells	569	3695	569
39	Retinal pigment cells	1451	4251	1451
40	Early Ectoderm 4	0	413	0

	Cell Type	DREAM	CorMotif	Hybrid
41	Amacrine cells	138	1104	138
42	Ductal cells	888	1976	888
43	Early Mesoderm 1	89	625	89
44	MUC13_DMBT1 positive cells	1358	3324	1358
45	Bronchiolar and alveolar epithelial cells	879	3950	879
46	Ganglion cells	381	1874	381
47	Thymic epithelial cells	353	1860	353
48	Horizontal cells	197	1506	197
49	Islet endocrine cells	2218	4293	2218
50	Granule neurons	450	1618	450
51	Unipolar brush cells	292	1103	292
52	Corneal and conjunctival epithelial cells	91	604	91
53	Mesothelial cells	1452	3120	1452
54	Antigen presenting cells	42	779	42
55	Neuroendocrine cells	340	1760	340
56	Stellate cells	323	1490	323
57	PDE1C_ACSM3 positive cells	206	1679	206
58	Photoreceptor cells	583	2596	583
59	Skeletal muscle cells	436	4718	436
60	Microglia	2233	5124	2233
61	SLC26A4_PAEP positive cells	1638	4633	1638
62	Erythroblasts	656	4622	656
63	Megakaryocytes	2118	5403	2118
64	Chromaffin cells	2	27	2
65	Extravillous trophoblasts	609	2950	609
66	ELF3_AGBL2 positive cells	7	410	7
67	CLC_IL5RA positive cells	0	429	0
68	Inhibitory interneurons	33	349	33
69	Lens fibre cells	463	2558	463
70	Sympathoblasts	522	4216	522
71	SATB2_LRRC7 positive cells	34	1119	34
72	Acinar cells	1509	4764	1509

Table S4. Number of differentially expressed genes by cell type. The number of differentially expressed cells calculated with DREAM at 5% false discovery rate, Cormotif and 95% posterior probability of DE, or in tetraploid hybrid cells using the Wilcoxon signed rank test at 5% false discovery rate.

	GO.ID	Term	p-value
1	GO:0008380	RNA splicing	0.00042
2	GO:0045931	positive regulation of mitotic cell cycl...	0.00044
3	GO:0006397	mRNA processing	0.00049
4	GO:0032007	negative regulation of TOR signaling	0.00197
5	GO:0006513	protein monoubiquitination	0.00212
6	GO:0043966	histone H3 acetylation	0.00294
7	GO:0051098	regulation of binding	0.00318
8	GO:0016236	macroautophagy	0.00392
9	GO:0016032	viral process	0.00433
10	GO:0000278	mitotic cell cycle	0.00515
11	GO:0016925	protein sumoylation	0.00552
12	GO:0032663	regulation of interleukin-2 production	0.00832
13	GO:0051028	mRNA transport	0.00951
14	GO:0006367	transcription initiation from RNA polyme...	0.01289
15	GO:0043161	proteasome-mediated ubiquitin-dependent ...	0.01318
16	GO:0000338	protein deneddylation	0.01594
17	GO:2000757	negative regulation of peptidyl-lysine a...	0.01594
18	GO:0043967	histone H4 acetylation	0.01598
19	GO:0006606	protein import into nucleus	0.01610
20	GO:0016567	protein ubiquitination	0.01703

Table S5. Gene Ontology enrichment in genes not differentially expressed in any cell type. The gene set was filtered for genes that had at least 100 UMIs detected across all individuals and replicates in at least 10 cell types. The top 20 terms are provided.

	pathway	p-value	Normalized enrichment score
1	TUBE_MORPHOGENESIS	9.8E-10	1.8
2	TUBE_DEVELOPMENT	2.2E-09	1.8
3	REGULATION_OF_MULTICELLULAR_ORGANISMAL_DEVELOPMENT	9.8E-09	1.7
4	CELL_FATE_COMMITMENT	1.1E-08	2.3
5	TISSUE_DEVELOPMENT	2.9E-08	1.6
6	ANIMAL_ORGAN_MORPHOGENESIS	4.2E-08	1.8
7	ANATOMICAL_STRUCTURE_FORMATION_INVOLVED_IN_MORP...	1.3E-07	1.7
8	EMBRYO_DEVELOPMENT	2.2E-07	1.7
9	ENZYME_LINKED_RECEPTOR_PROTEIN_SIGNALING_PATHWAY	2.2E-07	1.7
10	BIOLOGICAL_ADHESION	2.4E-07	1.6
11	REGULATION_OF_CELL_POPULATION_PROLIFERATION	6.0E-07	1.6
12	EMBRYONIC_ORGAN_DEVELOPMENT	6.5E-07	1.9
13	CELL_CYCLE	1.4E-06	1.5
14	EMBRYONIC_MORPHOGENESIS	2.0E-06	1.8
15	CIRCULATORY_SYSTEM_DEVELOPMENT	2.5E-06	1.6
16	EPITHELIUM_DEVELOPMENT	6.1E-06	1.6
17	REGULATION_OF_CELL_DIFFERENTIATION	6.1E-06	1.5
18	PATTERN_SPECIFICATION_PROCESS	1.2E-05	1.9
19	POSITIVE_REGULATION_OF_CELL_POPULATION_PROLIFER...	1.3E-05	1.7
20	POSITIVE_REGULATION_OF_DEVELOPMENTAL_PROCESS	1.5E-05	1.5

Table S6. Gene Ontology enrichment for *trans* genes. We ranked genes according to the mean *trans* proportion across all cell types with DE and ran gene set enrichment against Gene Ontology Biological Process terms. The top 20 terms are provided.

	pathway	p-value	Normalized enrichment score
1	TFT_LEGACY_TAATTA_CHX10_01	2.9E-06	1.74
2	TFT_LEGACY_CTTTGA_LEF1_Q2	5.5E-06	1.62
3	TFT_GTRD_HSD17B8_TARGET_GENES	5.0E-05	1.69
4	MIR_DB_MIR144_3P	1.9E-04	1.75
5	MIR_DB_MIR8485	5.8E-04	1.50
6	TFT_LEGACY_GGATTA_PITX2_Q2	5.8E-04	1.64
7	TFT_LEGACY_YCATTAA_UNKNOWN	5.8E-04	1.69
8	MIR_DB_MIR9_5P	6.5E-04	1.68
9	TFT_LEGACY_CEBPDELTA_Q6	1.1E-03	1.88
10	TFT_LEGACY_CEBPA_01	1.3E-03	1.86
11	TFT_LEGACY_HNF1_C	1.3E-03	1.90
12	TFT_LEGACY_CAGCTG_AP4_Q5	1.3E-03	1.43
13	TFT_LEGACY_AACTTT_UNKNOWN	1.3E-03	1.39
14	TFT_LEGACY_GGGTGGRR_PAX4_03	1.7E-03	1.42
15	TFT_LEGACY_WGGAATGY_TEF1_Q6	2.3E-03	1.72
16	TFT_LEGACY_RYTTCCTG_ETS2_B	2.6E-03	1.47
17	TFT_LEGACY_GATA1_05	3.0E-03	1.77
18	TFT_LEGACY_IRF7_01	3.1E-03	1.81
19	TFT_LEGACY_CAGGTA_AREB6_01	3.2E-03	1.52
20	MIR_DB_MIR4699_3P	3.2E-03	1.58

Table S7. Transcription factor target enrichment for *trans* genes. We ranked genes according to the mean *trans* proportion across all cell types with DE and ran gene set enrichment against transcription factor targets. The top 20 terms are provided.

Data S1-S2

Data S1. Results of DREAM, Cormotif, Hybrid DE, and cis proportion. This supplementary data file is a flat tab-separated text file with the following columns defined:

gene	The gene symbol for the tested gene.
cell.type	The reference cell type the gene was tested in (see materials and methods).
layer	The inferred germ later of this cell type.
numi.human	The number of UMIs detected across all human individuals and replicates.
numi.chimp	The number of UMIs detected across all chimpanzee individuals and replicates.
dream.mean.human	Mean gene expression across humans, calculated by DREAM. UMI counts are log2 transformed as well as cyclicloess and TMM normalized.
dream.mean.chimp	Mean gene expression across chimpanzees, calculated by DREAM. UMI counts are log2 transformed as well as cyclicloess and TMM normalized.
dream.logFC	The log2 fold-change (the effect size) in gene expression in humans relative to chimpanzees, calculated by DREAM.

dream.SE	The standard error in the DREAM effect size estimate.
dream.mean	The mean expression of this gene across both humans and chimpanzees, as calculated by DREAM. UMI counts are log2 transformed as well as cyclicloess and TMM normalized.
dream.p.val	The raw p-value computed by DREAM.
dream.adj.pval	The Benjamini-Hochberg adjusted p-value, computed by DREAM.
cormotif.posterior	The posterior probability of differential expression, computed by Cormotif.
hybrid.numi.human	The number of human-assigned UMIs detected across all replicates of tetraploid human/chimpanzee hybrid cells.
hybrid.numi.chimp	The number of chimpanzee-assigned UMIs detected across all replicates of tetraploid human/chimpanzee hybrid cells.
hybrid.logFC	The hybrid effect size. Computed as the difference between log2(hybrid.numi.human + 1) and log2(hybrid.numi.human + 1). The pseudocount is included to prevent taking the logarithm of zero.
hybrid.p.val	The p-value of the difference between human and chimpanzee assigned counts, computed using a paired Wilcoxon signed-rank test .
hybrid.adj.pval	The Benjamini-Hochberg adjusted p-value in for the hybrid test.
cisprop	The estimated *cis* proportion of this change. Calculated as abs(hybrid.logFC) / (abs(dream.logFC – hybrid.logFC) + abs(hybrid.logFC))

Data S2. Genes with cell-type restricted differential expression. Raw text file containing the gene symbol of each gene with cell-type-restricted differential expression. One gene is listed per line.